

Efficient Techniques for Fluid Structure Interaction: Compatibility Coupling and Galerkin Differences

Jeff Banks

Rensselaer Polytechnic Institute

FEM@LLNL Sminar
July 26, 2022

Collaborators

Bill Henshaw, Don Schwendeman, Brett Buckner

Department of Mathematical Sciences

Rensselaer Polytechnic Institute

Jason Hicken, Ge Yan, Sharanjeet Kaur

Mechanical Engineering

Rensselaer Polytechnic Institute

Qi Tang, Dan Serino

Applied Mathematics and Plasma Physics Group

Los Alamos National Laboratory

Tom Hagstrom

Southern Methodist University

Support

Department of Energy

Office of Advanced Scientific Computing Research

Applied Mathematics Program

NNSA

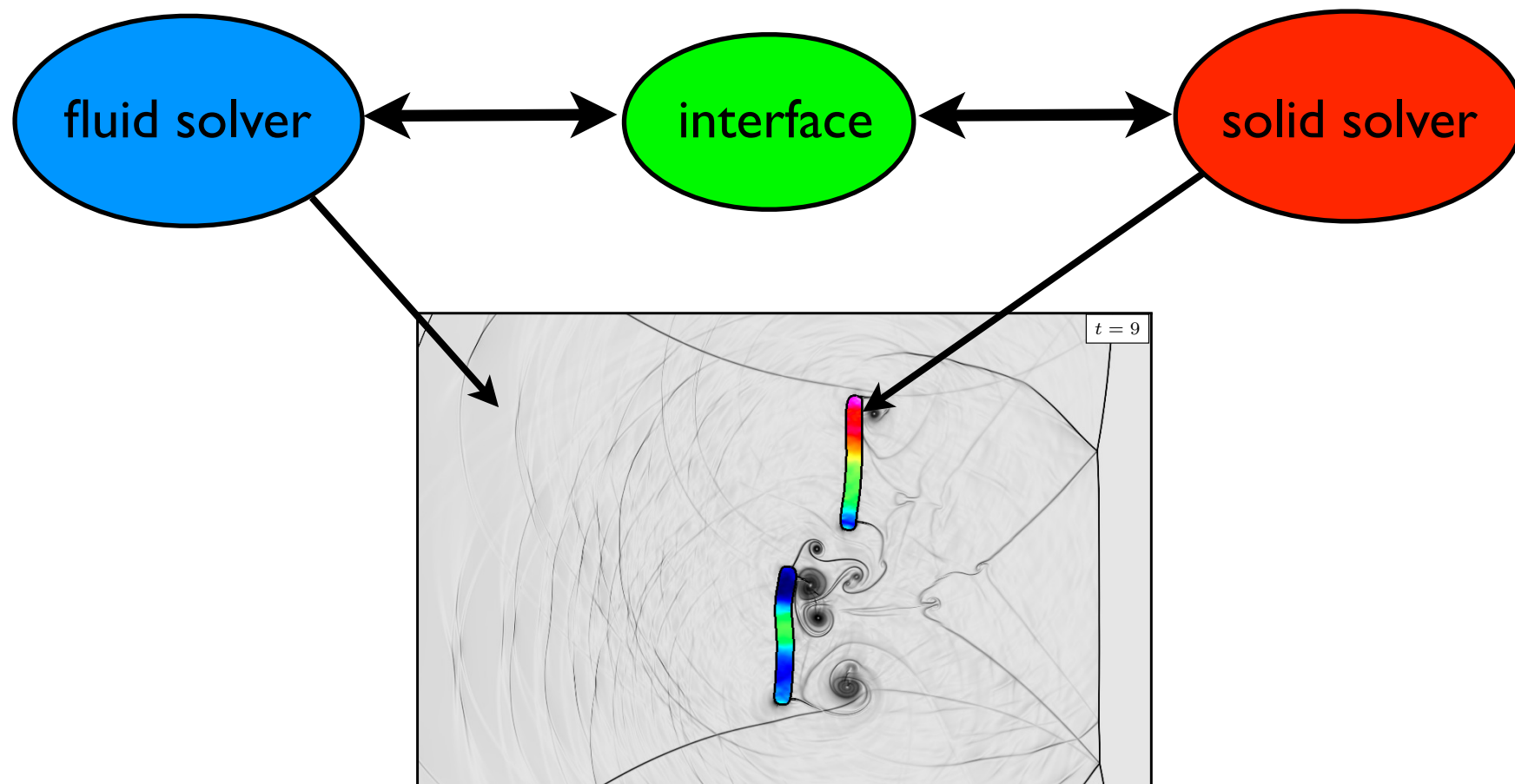
National Science Foundation

Division of Mathematical Sciences

Lawrence Livermore National Laboratory

Rensselaer Polytechnic Institute

At a high level, this talk focuses on partitioned FSI solvers which are ideally suited to modern high-performance computation



- Component solvers remain independent
 - can use existing solvers
 - no need to solve (or precondition) a coupled implicit system
- Can naturally take advantage of disparate time scales
 - e.g. mixing implicit and explicit integration
- High levels of algorithmic concurrency
 - maps well to modern and emerging computers

Traditional partitioned schemes have suffered from “added-mass instabilities” for solids which are sufficiently light when compared to the fluid

- Traditional partitioned FSI algorithms (Cirak, et. al. 2007, Bungartz and Schafer 2006)
 1. advance fluid (using interface velocity/displacement from the solid)
 2. advance solid (apply fluid forces to the solid)
 3. possibly iterate with under-relaxation to convergence

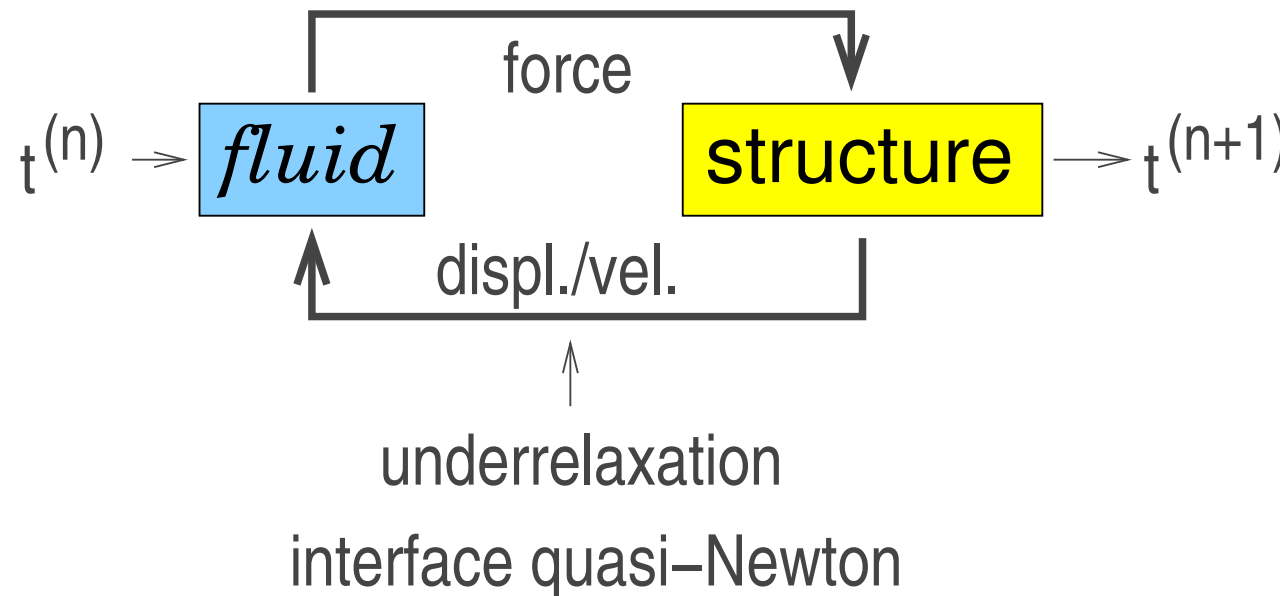
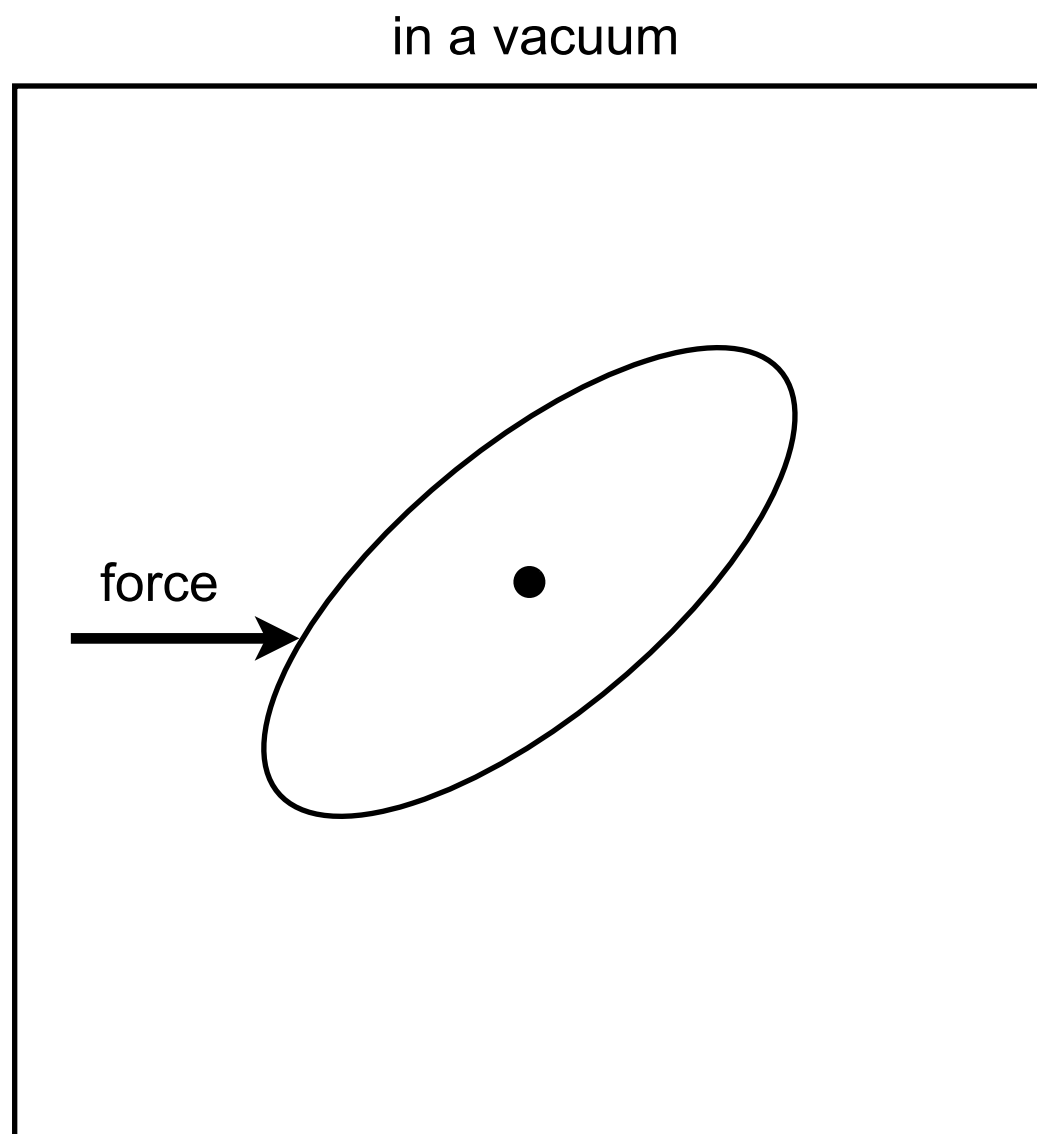


diagram from
Keyes et. al. 2012

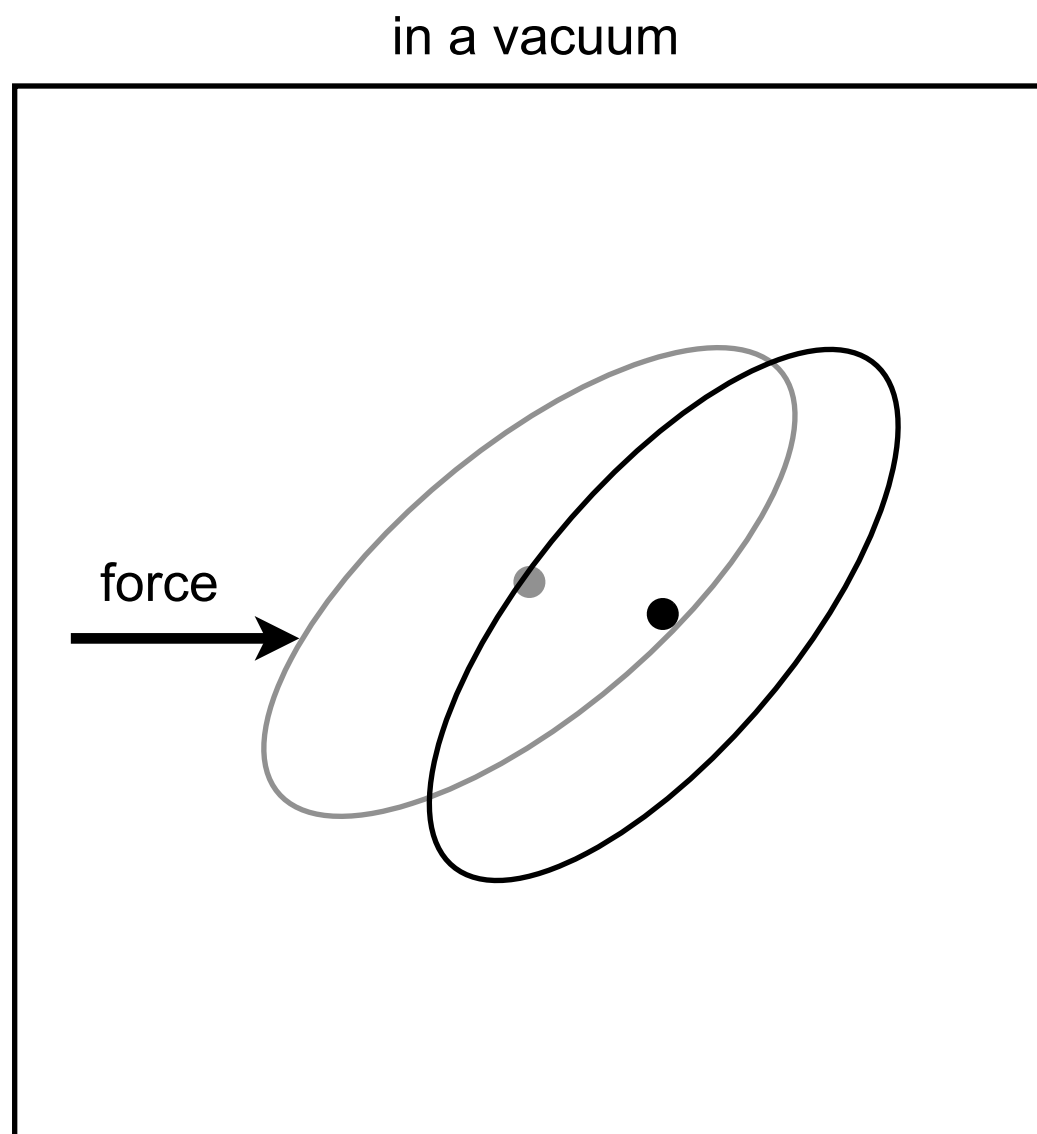
- Some analysis of added-mass instabilities can be found in the literature, for example
 - Causin, Grebeau, and Nobile, 2005 (stability with relaxation)
 - Gretarsson, Kwatra, and Fedkiw 2011 (semi-monolithic formulations)

The origin of added-mass instabilities is that the effect of displaced fluid is not appropriately accounted for in the numerical algorithms



Body simply moves according to
Newton's laws of motion

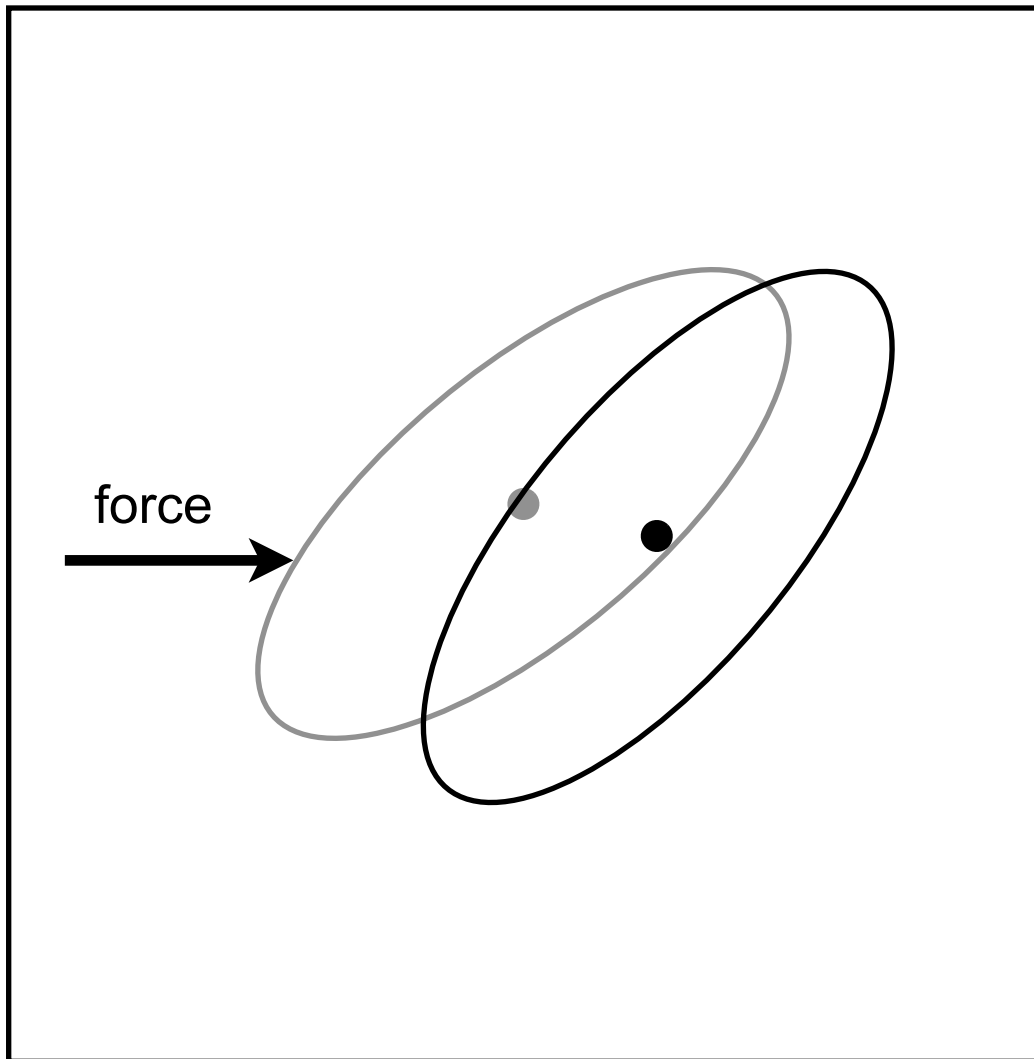
The origin of added-mass instabilities is that the effect of displaced fluid is not appropriately accounted for in the numerical algorithms



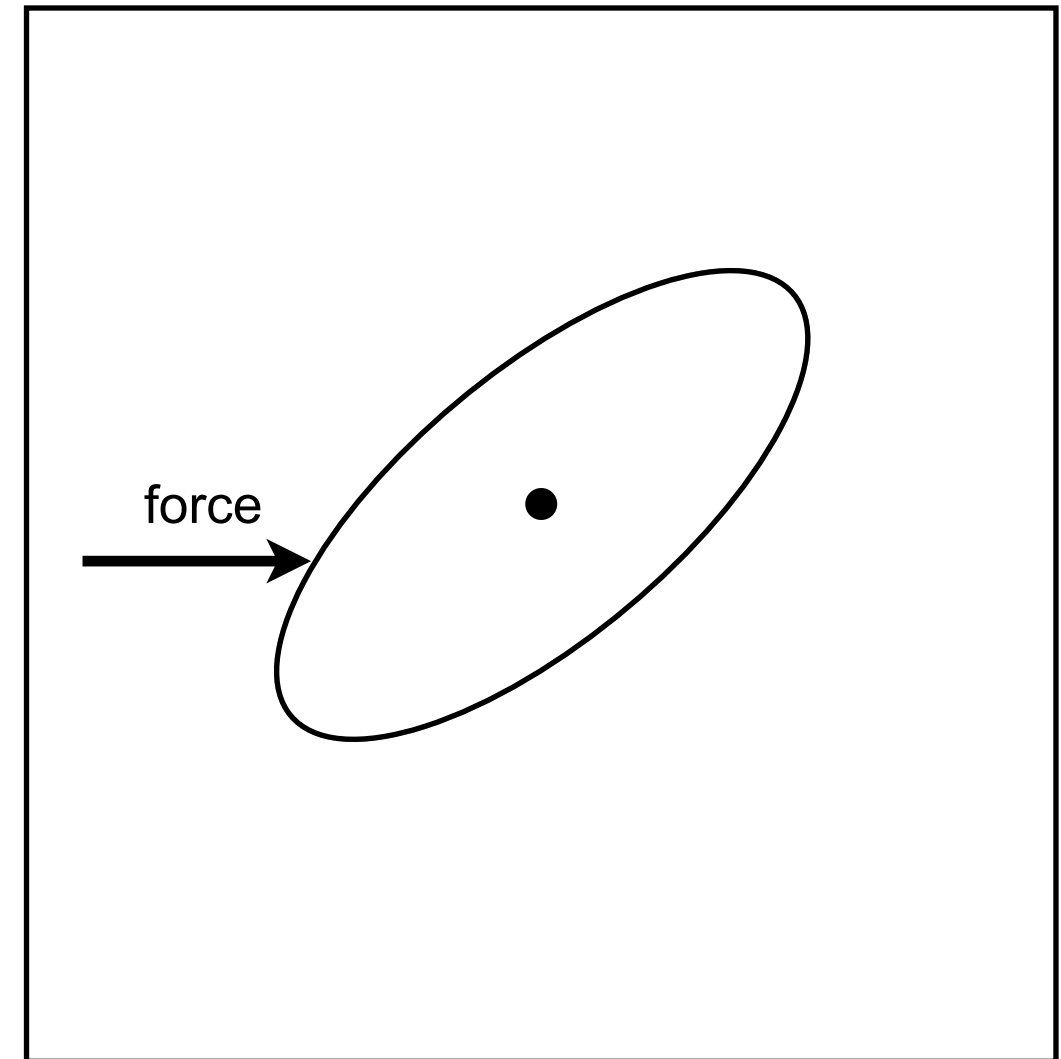
Body simply moves according to
Newton's laws of motion

The origin of added-mass instabilities is that the effect of displaced fluid is not appropriately accounted for in the numerical algorithms

in a vacuum



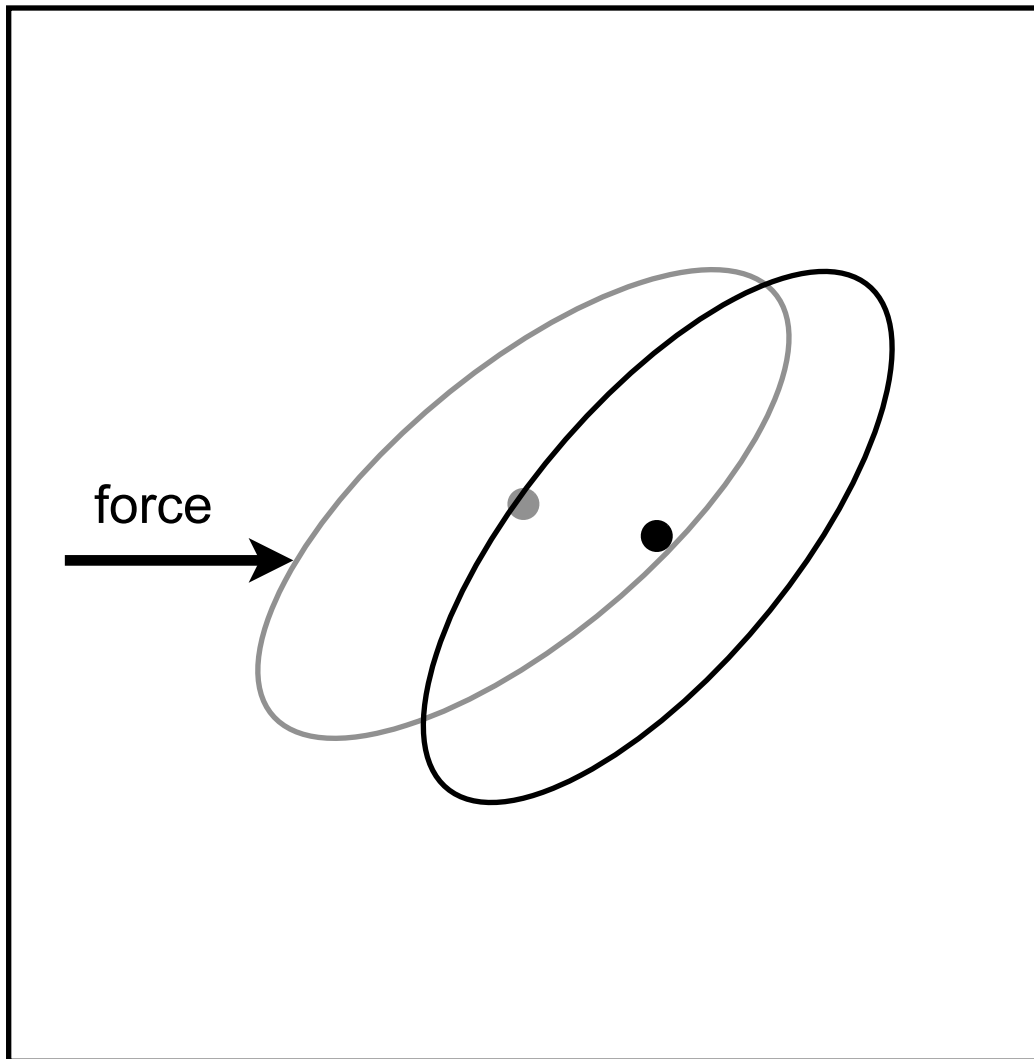
in a fluid



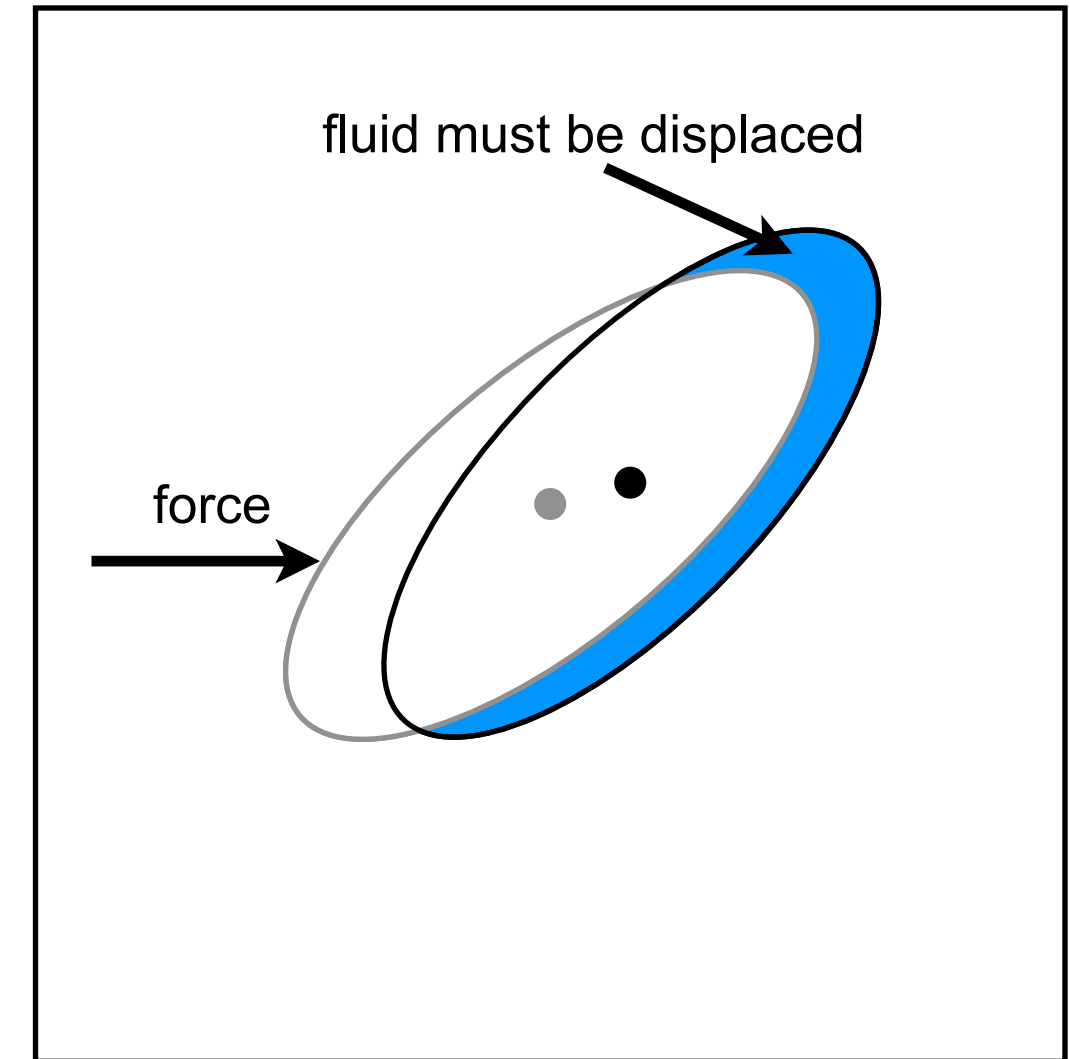
Body simply moves according to
Newton's laws of motion

The origin of added-mass instabilities is that the effect of displaced fluid is not appropriately accounted for in the numerical algorithms

in a vacuum



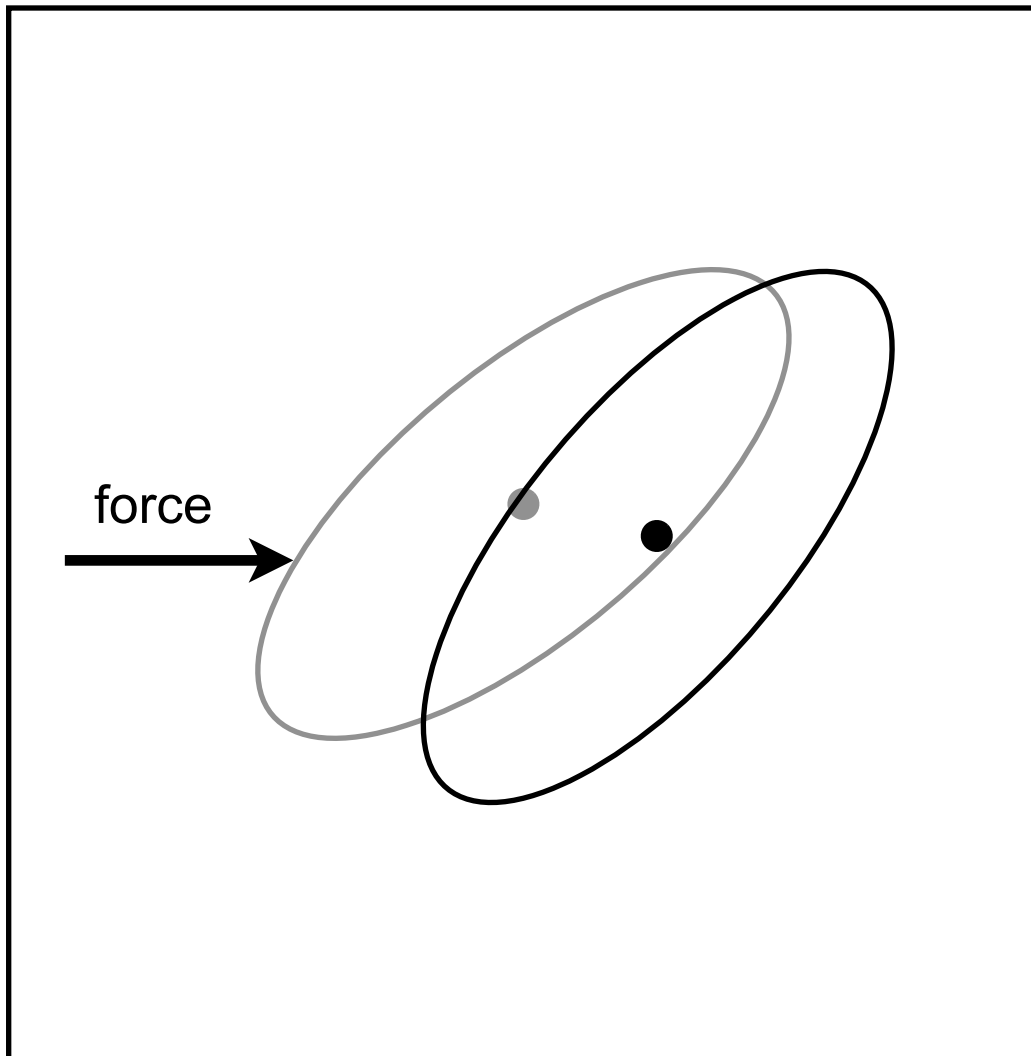
in a fluid



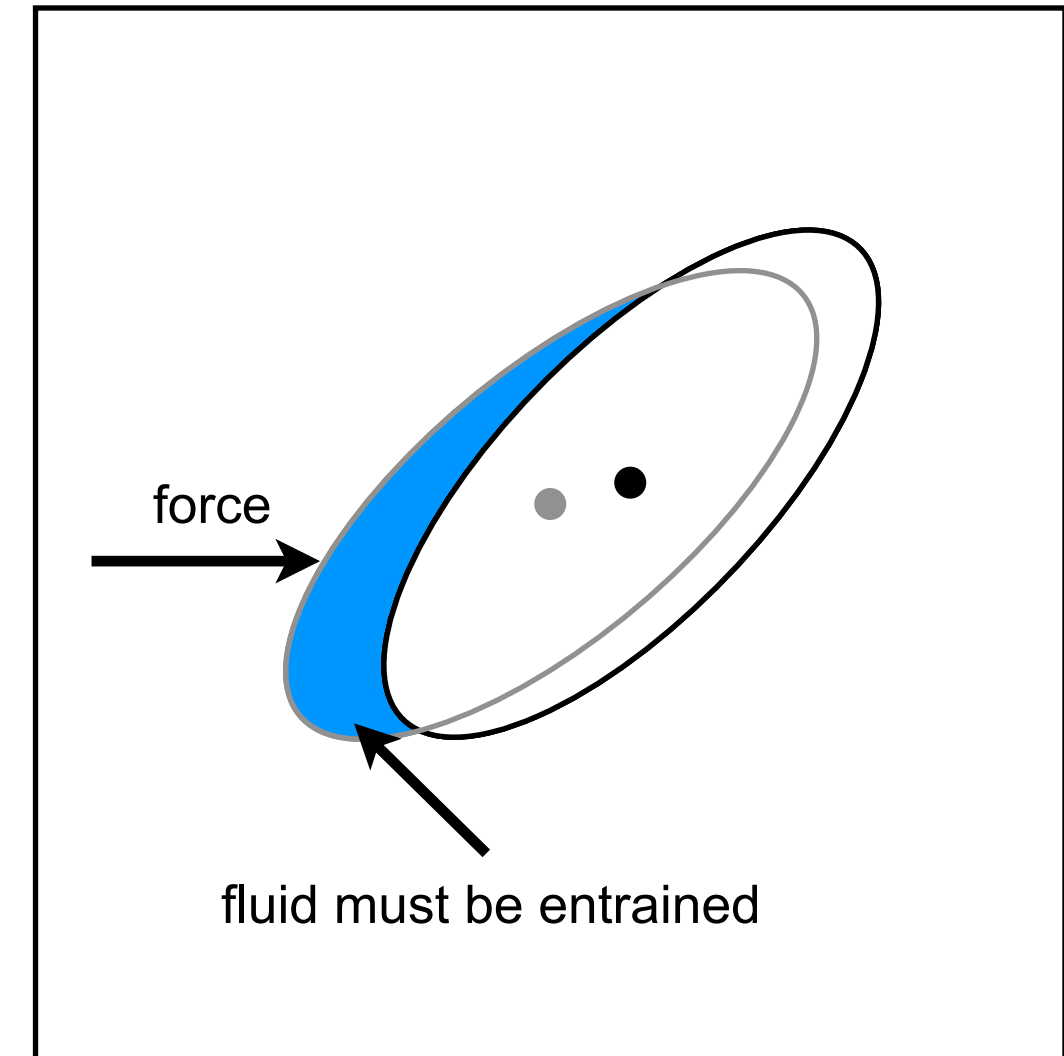
Body simply moves according to
Newton's laws of motion

The origin of added-mass instabilities is that the effect of displaced fluid is not appropriately accounted for in the numerical algorithms

in a vacuum



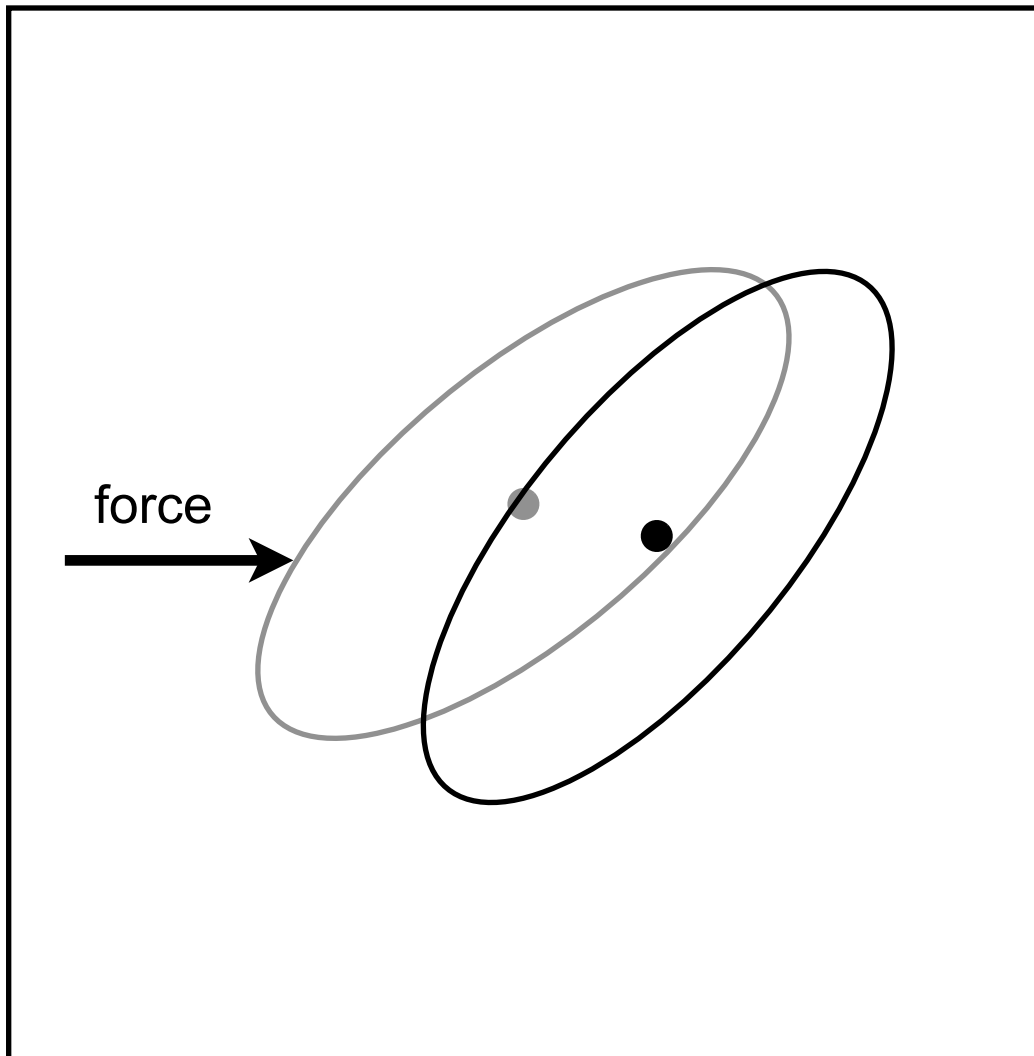
in a fluid



Body simply moves according to
Newton's laws of motion

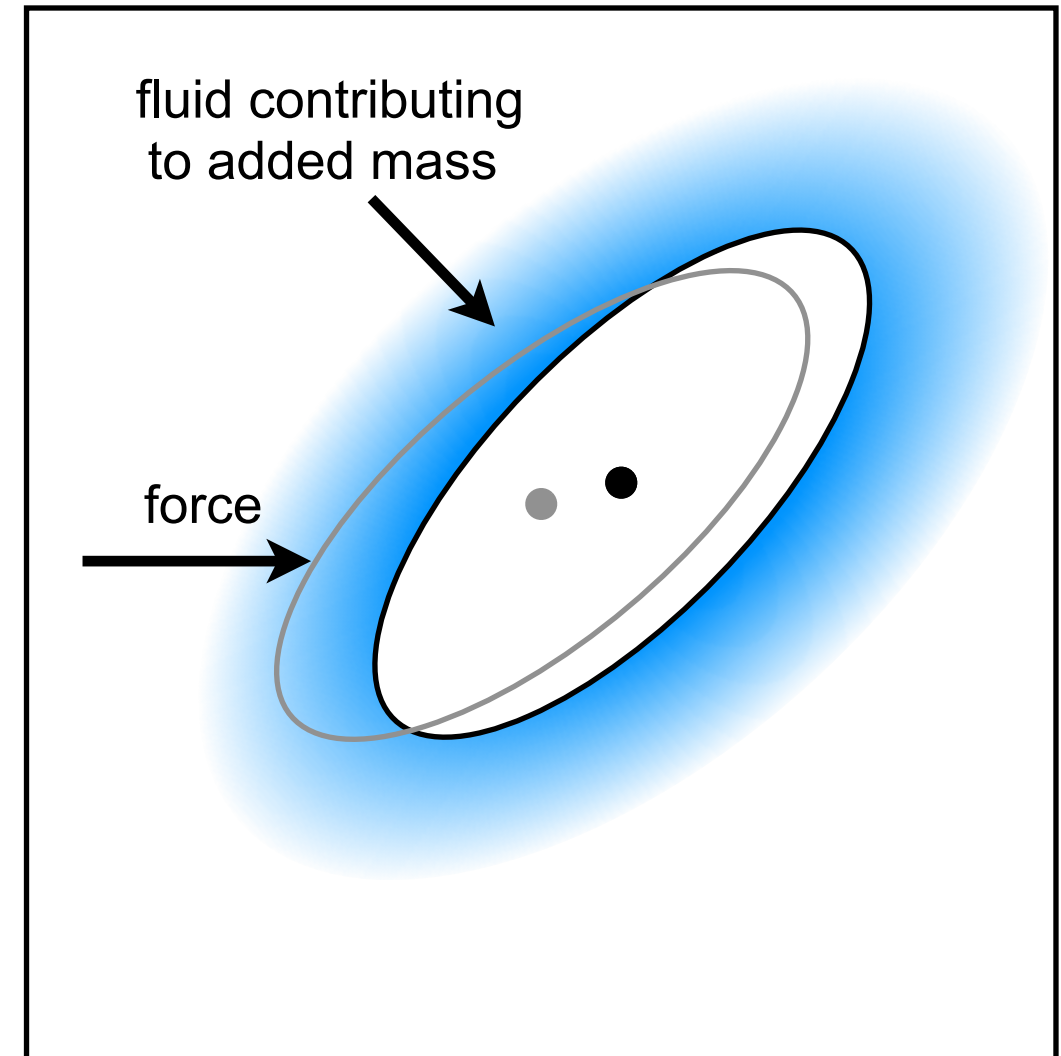
The origin of added-mass instabilities is that the effect of displaced fluid is not appropriately accounted for in the numerical algorithms

in a vacuum



Body simply moves according to
Newton's laws of motion

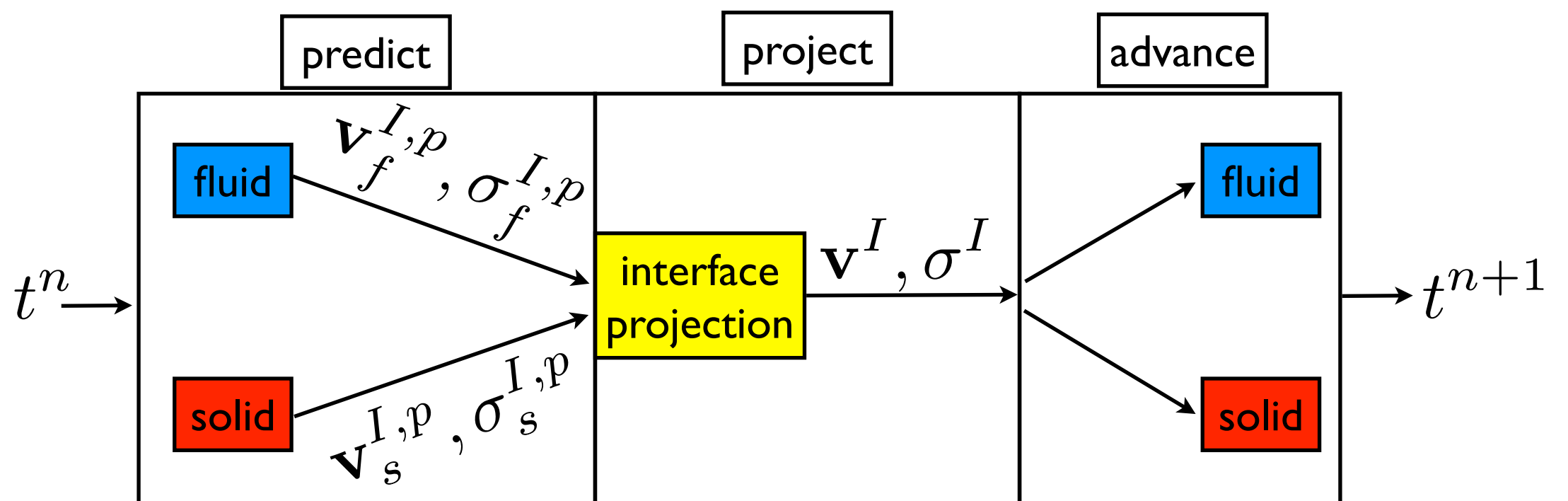
in a fluid



Body must displace and entrain fluid to move
and therefore appears more massive than in
vacuum ... the so called "added mass"

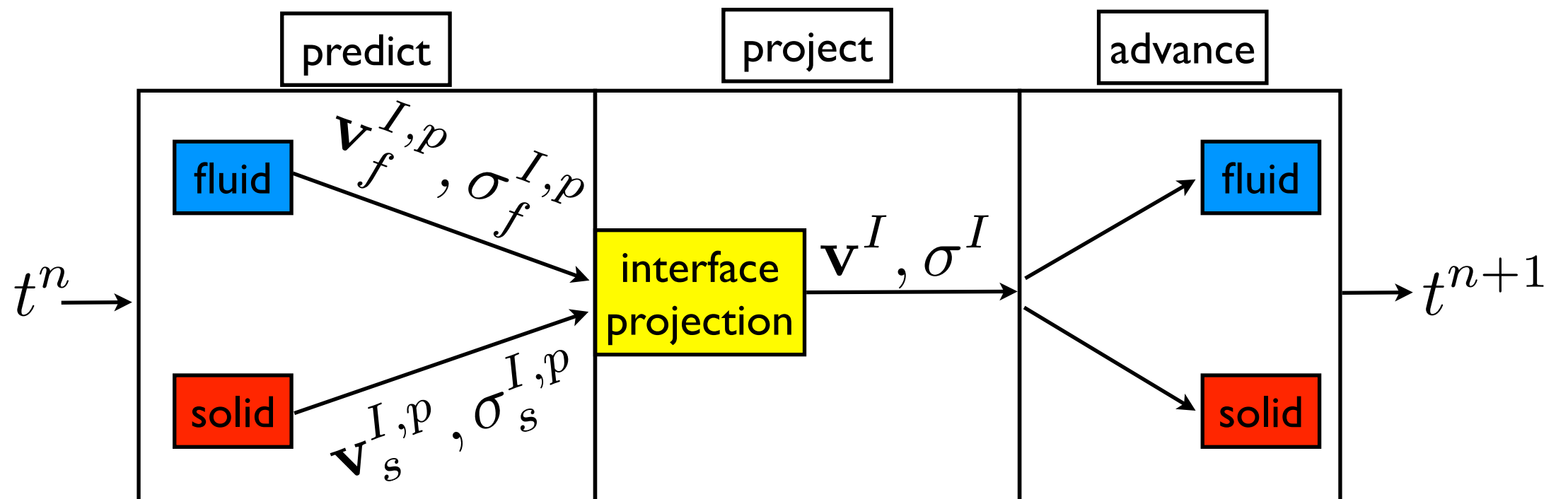
To account for the strongly coupled nature of FSI interface dynamics,
we have developed the idea of an “interface projection”

- At the continuous level, the interface velocity and stress are defined in terms of the coupled fluid/solid problem
- The job of the interface projection is to define the solution at the interface in terms of (disparate) predictions from the fluid and solid
- The resultant interface dynamics are then imposed on the fluid and solid domains



To account for the strongly coupled nature of FSI interface dynamics, we have developed the idea of an “interface projection”

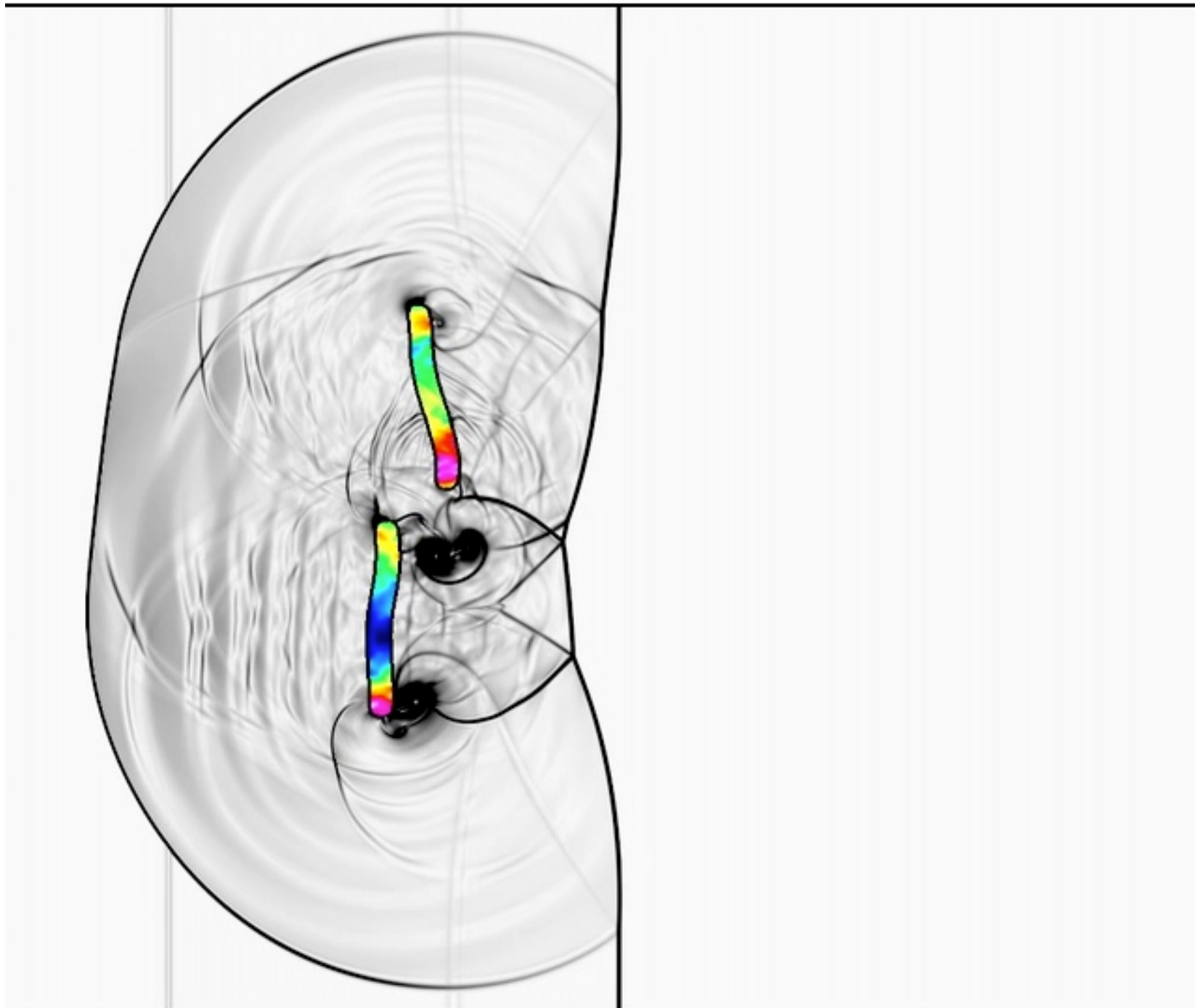
- At the continuous level, the interface velocity and stress are defined in terms of the coupled fluid/solid problem
- The job of the interface projection is to define the solution at the interface in terms of (disparate) predictions from the fluid and solid
- The resultant interface dynamics are then imposed on the fluid and solid domains



- The resulting schemes will be called **Added-Mass Partitioned (AMP)**

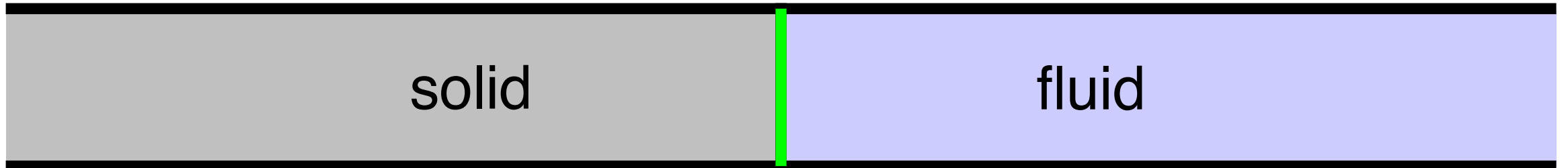
As a concrete motivating example consider shock structure interaction

- High-speed compressible fluids (Euler equations)
- Compressible elastic solids (linear or nonlinear elasticity)



Example: Mach-2 shock impacting deformable sticks

To understand the dynamics of the interface it is useful to simplify and consider a 1D model problem



Linear Elasticity

$$\begin{cases} \partial_t \bar{u} - \bar{v} = 0 \\ \bar{\rho} \partial_t \bar{v} - \partial_{\bar{x}} \bar{\sigma} = 0 \\ \partial_t \bar{\sigma} - \bar{\rho} c_p^2 \partial_{\bar{x}} \bar{v} = 0 \end{cases}$$

Euler Equations

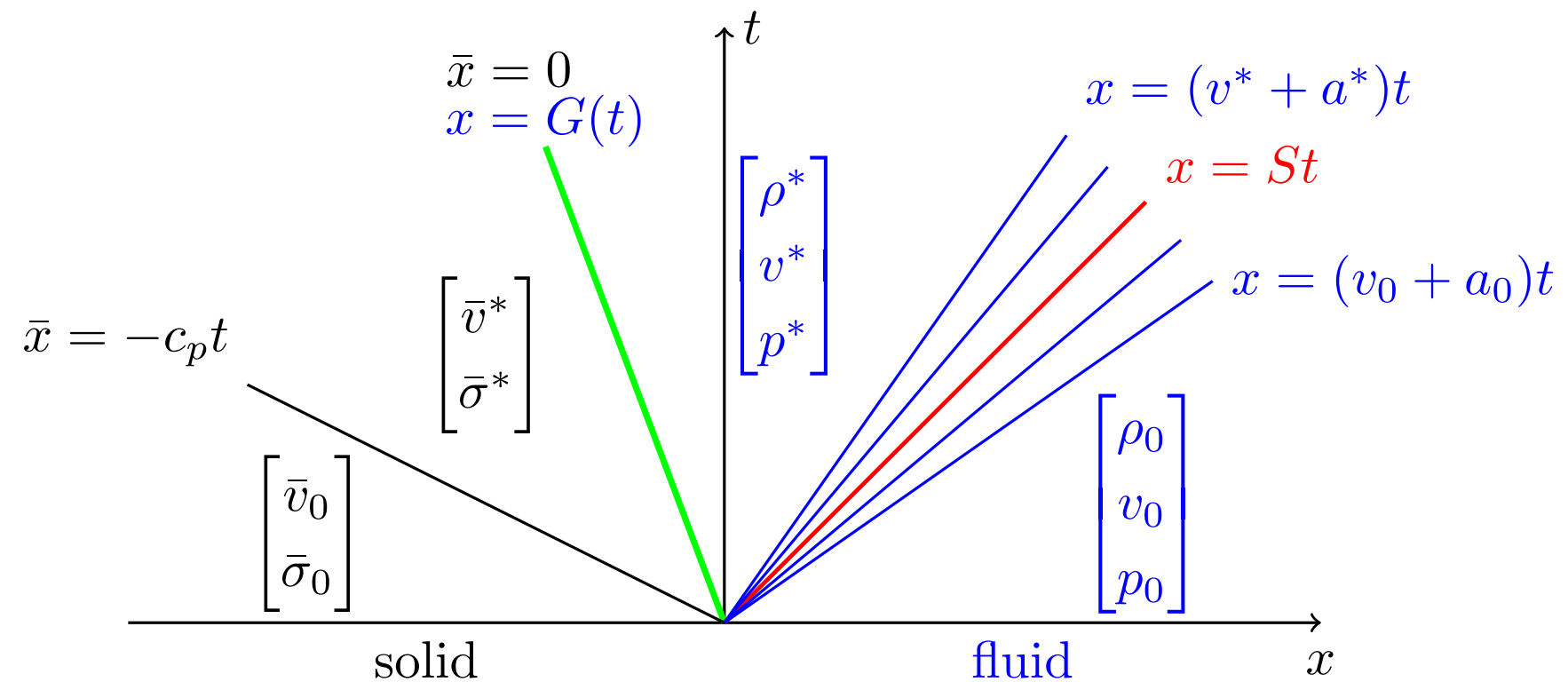
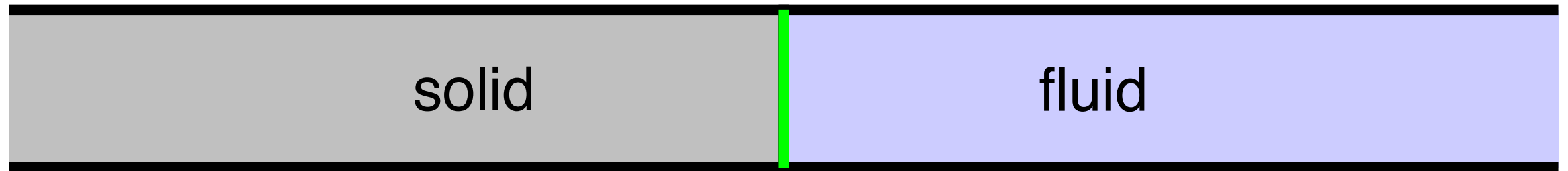
$$\begin{cases} \partial_t \rho + \partial_x (\rho v) = 0 \\ \partial_t (\rho v) + \partial_x (\rho v^2 + p) = 0 \\ \partial_t (\rho E) + \partial_x (\rho E v + p v) = 0 \end{cases}$$

Interface Coupling Conditions

$$\begin{cases} \bar{v}(\bar{x}, t) = v(x, t), \\ \bar{\sigma}(\bar{x}, t) = \sigma(x, t) \equiv -p(x, t) + p_e \end{cases}$$

Greengard's Axiom: “It never hurts to start by writing down the exact solution to the problem”

We localize near the interface, and obtain a fluid structure Riemann problem (FSRP) whose solution can be used for FSI coupling



- This is a specific case of the elastic piston problem with constant states
- Exact solutions to the linear and nonlinear problem can be found

Our added-mass partitioned (AMP) schemes use **compatibility interface conditions** and embed solutions to the FSRP as discrete interface conditions

- Along the interface, the solution is projected using solutions to local FSRPs

$$v_I = \frac{\bar{z}\bar{v}_0 + zv_0}{\bar{z} + z} + \frac{\sigma_0 - \bar{\sigma}_0}{\bar{z} + z}$$

$$\sigma_I = \frac{\bar{z}^{-1}\bar{\sigma}_0 + z^{-1}\sigma_0}{\bar{z}^{-1} + z^{-1}} + \frac{v_0 - \bar{v}_0}{\bar{z}^{-1} + z^{-1}}$$

$$\rho_I = \rho_0(p_I/p_0)^{1/\gamma}$$

- The traditional FSI coupling is the large impedance (mass) limit $\bar{z} \gg z$
 - velocity from solid $v_I = \bar{v}_0$
 - stress from fluid $\sigma_I = \sigma_0 = -p_0 + p_e$
- Here $\bar{z} = \bar{\rho}c_p$ and $z = \rho_0a_0$ are acoustic impedances

The stability of the discretization varies significantly based on the formulation of discrete interface conditions

Theorem: For the first-order upwind method and the interface conditions given by

$$\begin{bmatrix} v_I \\ \sigma_I \end{bmatrix}^n = \frac{1}{z_L + z_R} \begin{bmatrix} z_L v_L + z_R v_R + (\sigma_R - \sigma_L) \\ z_R \sigma_L + z_L \sigma_R + z_R z_L (v_R - v_L) \end{bmatrix}_0^n$$

the discretization is stable under the constraint $\lambda = \frac{c\Delta t}{\Delta x} < 1$

Theorem: For first-order upwind methods and the interface conditions that take the velocity from the left and the stress from the right

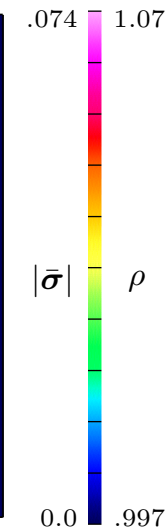
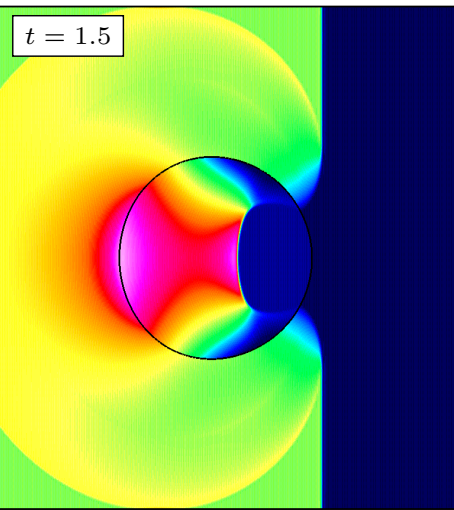
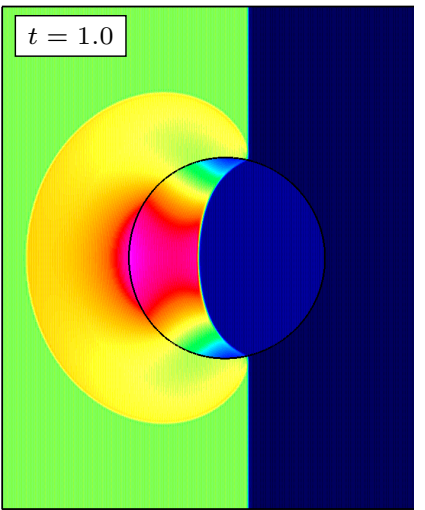
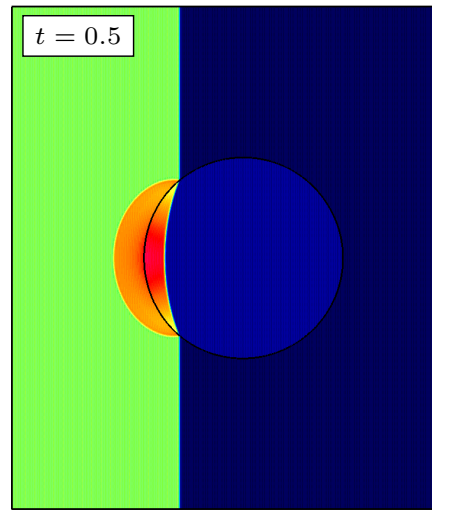
$$\begin{bmatrix} v_I \\ \sigma_I \end{bmatrix}^n = \begin{bmatrix} v_L \\ \sigma_R \end{bmatrix}_0^n$$

the discretization is stable under the constraint $\lambda = \frac{c\Delta t}{\Delta x} < \min \left(1, \frac{4}{1 + \frac{\rho_R}{\rho_L}} \right)$

Thus for $\rho_R < 3\rho_L$ the discretization is stable under the standard CFL limit. The maximum stable time step decreases to zero as the density ratio increases.

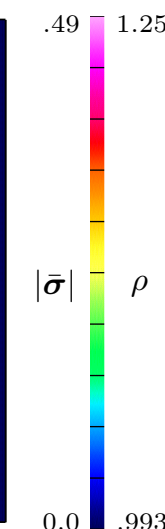
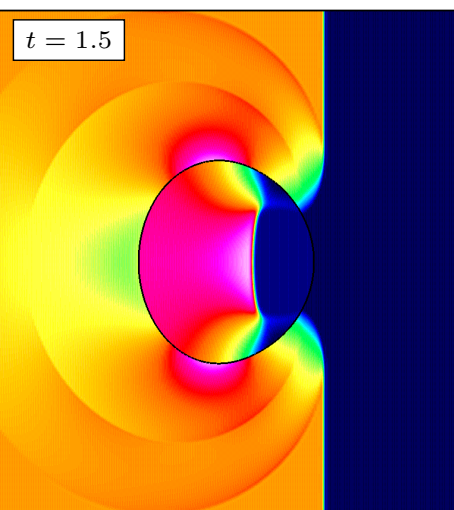
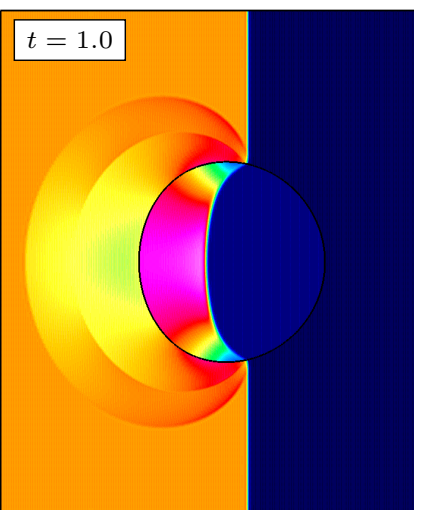
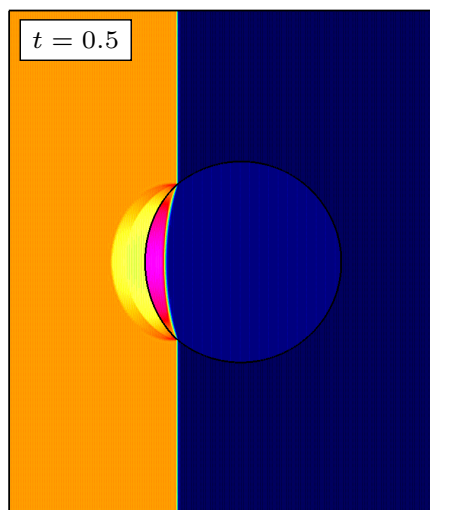
Stability of AMP solver for a variety of fluid/solid densities is demonstrated

(example of solid compression wave impacting fluid cavity)



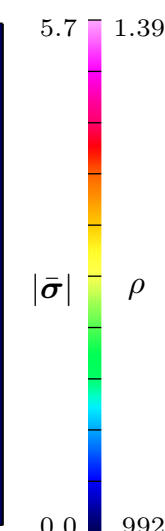
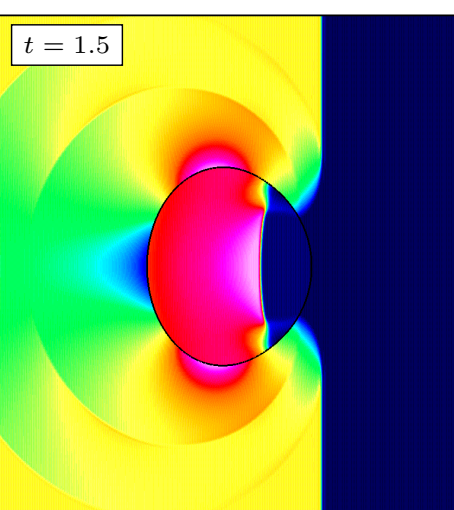
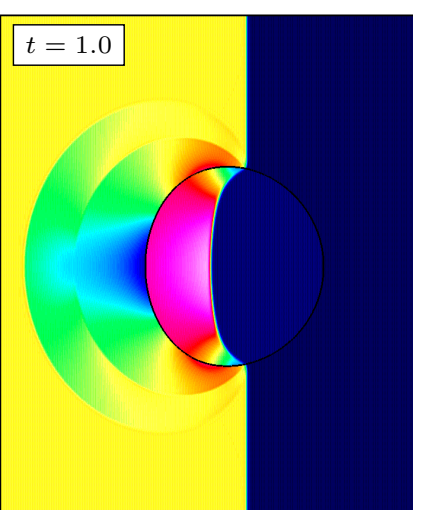
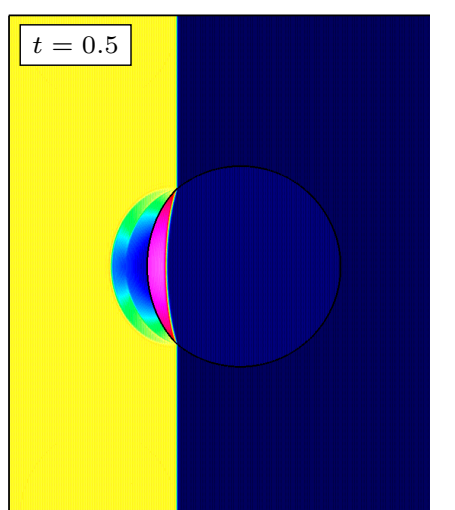
light solid
 $\bar{\rho} = 0.1$

Traditional coupling fails!



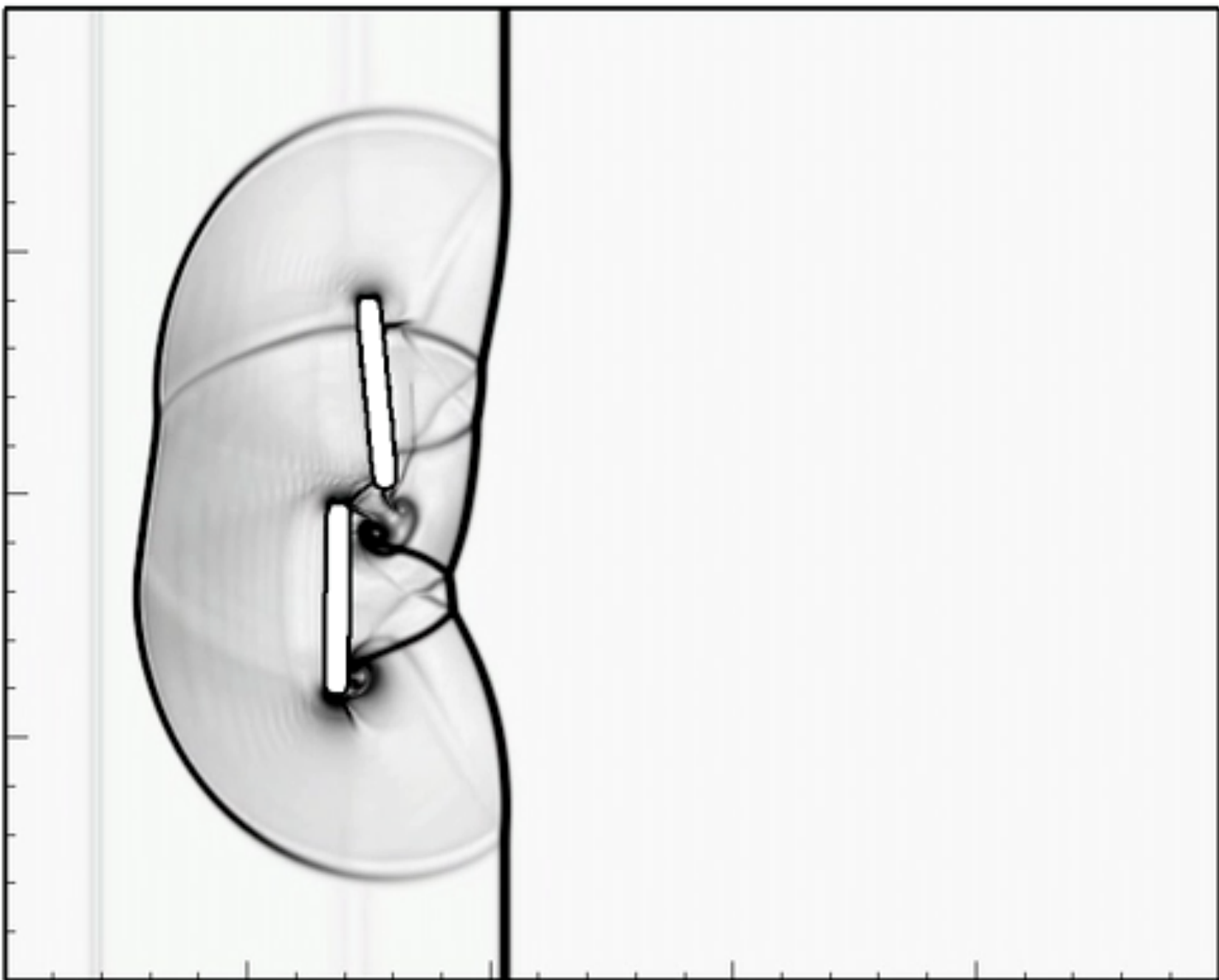
medium solid
 $\bar{\rho} = 1.0$

Traditional coupling fails!



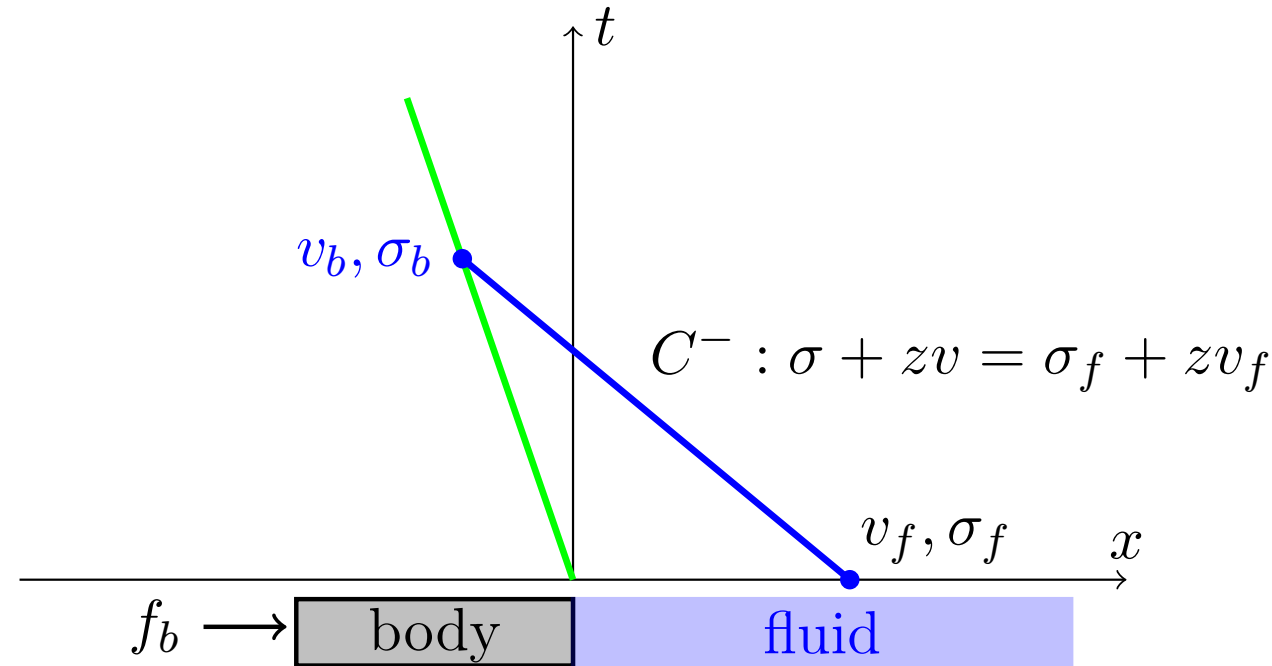
heavy solid
 $\bar{\rho} = 10.0$

For other regimes, the situation is potentially more challenging, e.g. what if we simply replace the deforming bodies with rigid objects?



Example: Mach-2 shock impacting rigid sticks

For rigid bodies the principle of compatibility interface conditions is the same, but the details and consequences are more subtle



Newton's law of motion

$$\begin{aligned} m_b \dot{v}_b &= \sigma_b + f_b, \\ \dot{x}_b &= v_b \end{aligned}$$

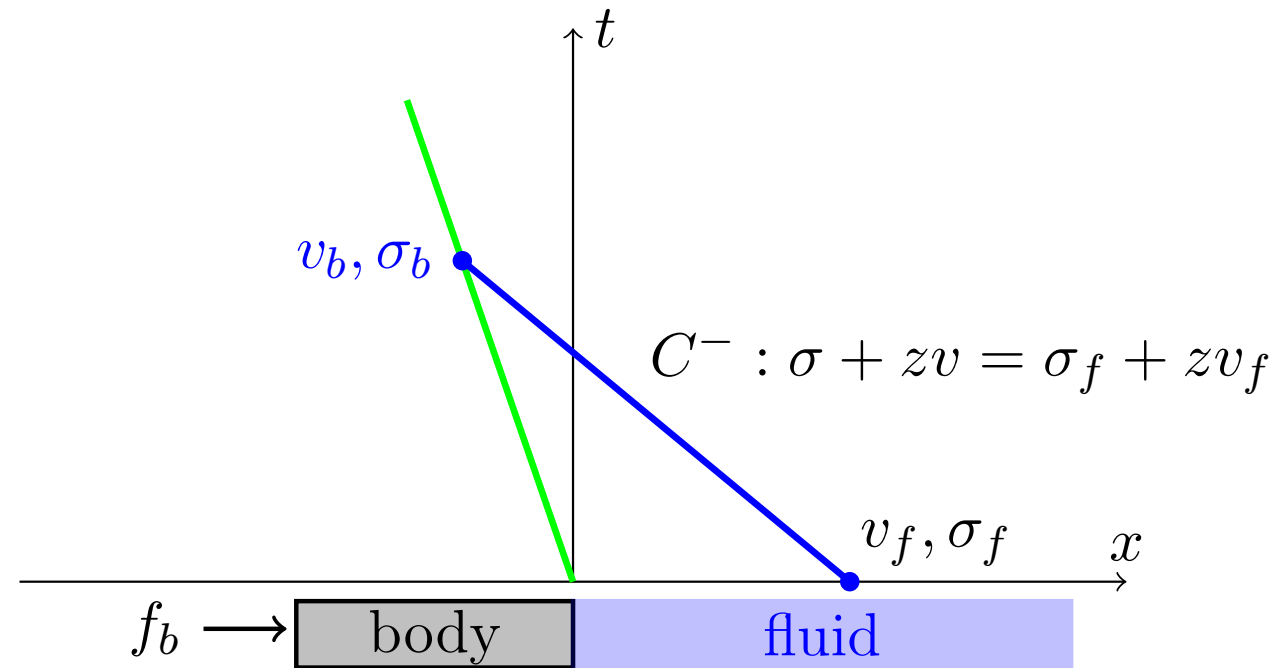
Linearized Euler equations

$$\left\{ \begin{array}{l} \partial_t \rho + \hat{v} \partial_x \rho + \hat{\rho} \partial_x v = 0 \\ \partial_t v + \hat{v} \partial_x v - (1/\hat{\rho}) \partial_x \sigma = 0 \\ \partial_t \sigma + \hat{v} \partial_x \sigma - \hat{\rho} \hat{c}^2 \partial_x v = 0 \end{array} \right.$$

- From the theory of characteristics we obtain the stress on the body

$$\sigma_b = \sigma_f + z(v_f - v_b)$$

The projected force correctly exposes the dependence of the applied stress on the motion of the body, and thereby reveals the “added mass”



$$\sigma_b = \sigma_0 + z(v_0 - v_b)$$

- We have exposed the dependence of the applied stress on the velocity of the body
- Therefore the equations of motion are well-defined even for zero mass

$$m_b \dot{v}_b + \boxed{zv_b} = \sigma_0 + zv_0 + f_b(t)$$

- The added mass term occurs naturally and reflects the effect of displaced fluid

The stability of the new AMP scheme is seen to be significantly better than the traditional scheme

Theorem: For the first-order upwind scheme for fluid domains, the backward Euler integrator for the rigid body, and the new projection

$$\sigma_b = \sigma_f + z(v_f - v_b)$$

the discrete system is stable for $m_b \geq 0$ and $\lambda = \frac{c\Delta t}{\Delta x} < 1$

Theorem: For the first-order upwind scheme for fluid domains, the backward Euler integrator for the rigid body, and the traditional projection

$$\sigma_b = \sigma_f$$

the discrete system is stable for $\lambda = \frac{c\Delta t}{\Delta x} < 1$ and $\Delta t < m_b(4 - \lambda)/(\rho c \lambda)$

Incorporating the AMP projection in the 2D or 3D equations of motion is straight forward and the result reveals added mass tensors

- In 2D the equations of motion are

$$m_b \dot{\mathbf{v}}_b = \mathcal{F},$$
$$A\dot{\boldsymbol{\omega}} = -WA\boldsymbol{\omega} + \mathcal{T}$$

- After some manipulation the added-mass is revealed

$$m_b \dot{\mathbf{v}}_b + \boxed{A^{vv}} \mathbf{v}_b + \boxed{A^{v\omega}} \boldsymbol{\omega} = \tilde{\mathcal{F}},$$
$$A\dot{\boldsymbol{\omega}} + \boxed{A^{\omega v}} \mathbf{v}_b + \boxed{A^{\omega\omega}} \boldsymbol{\omega} = \tilde{\mathcal{T}}$$

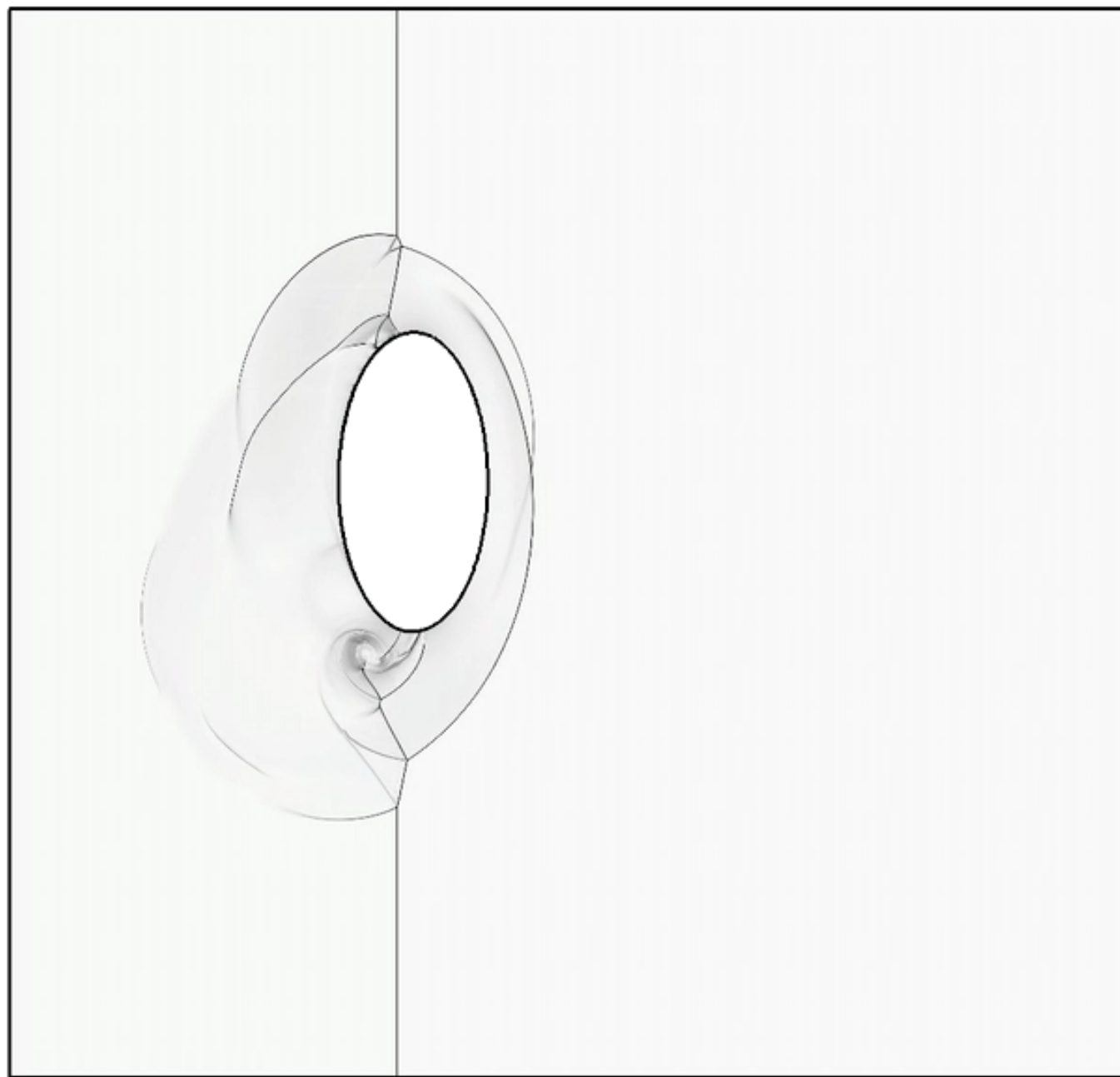
- Where the added mass tensors are expressed as surface integrals, for example

$$A^{vv} = \int_{\partial B} z_f \mathbf{n} \mathbf{n}^T \, ds$$

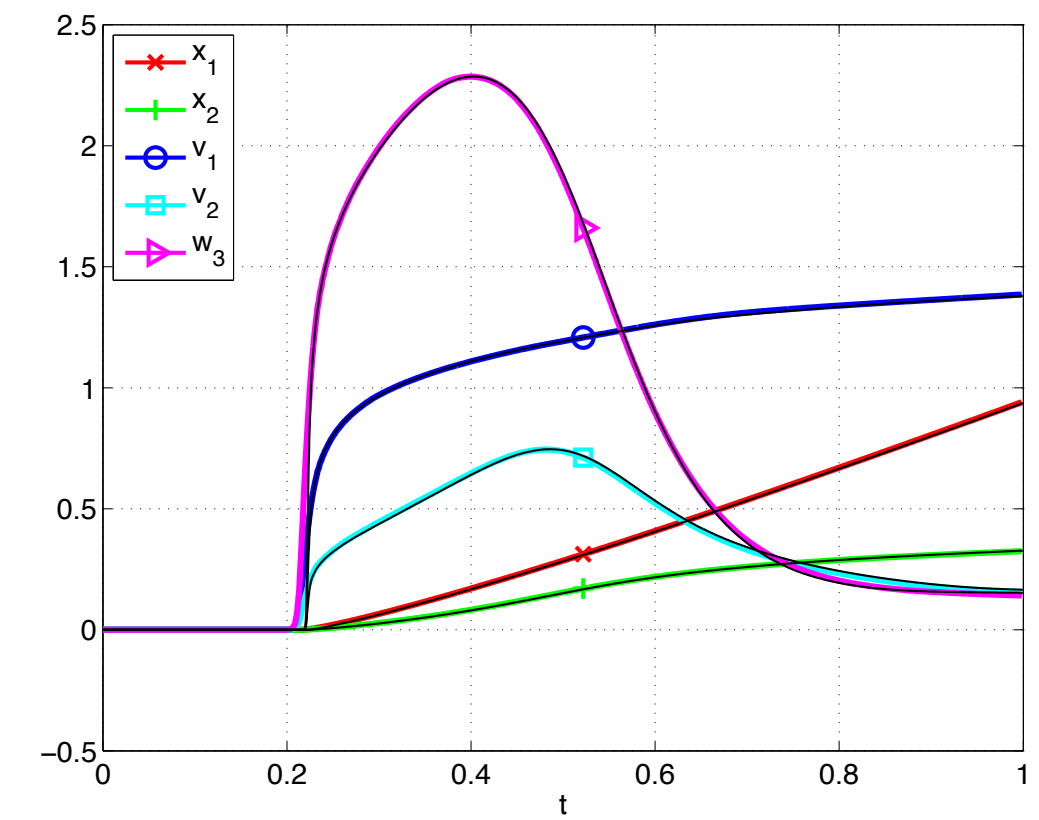
- Definitions for the analytic forms of the added mass tensors for compressible flow was an open question (Love 1905, Taylor 1942)

The AMP-FSI algorithm is accurate and stable even for a zero mass rigid body

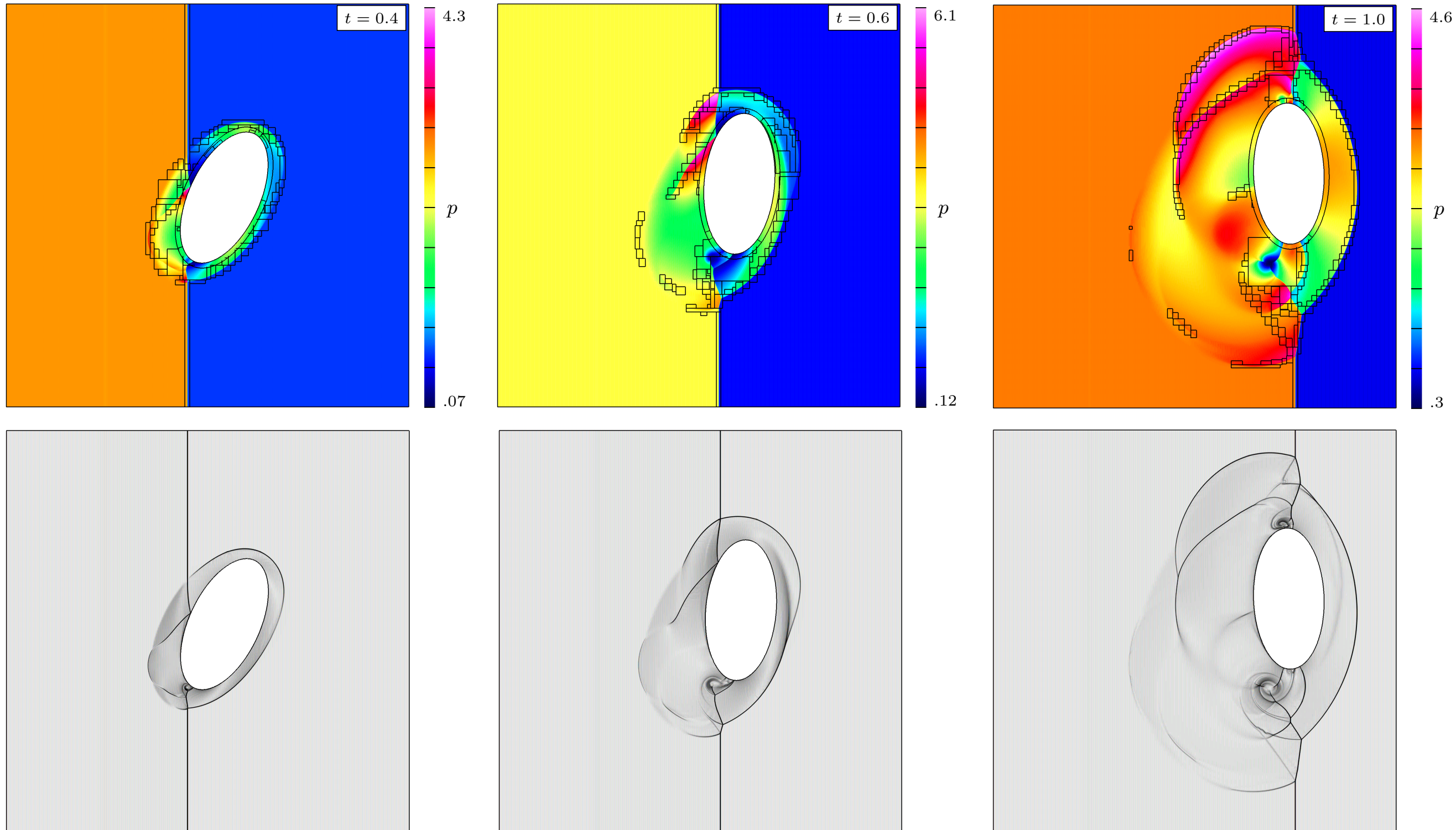
Mach 2 shock impacting zero mass body with AMR



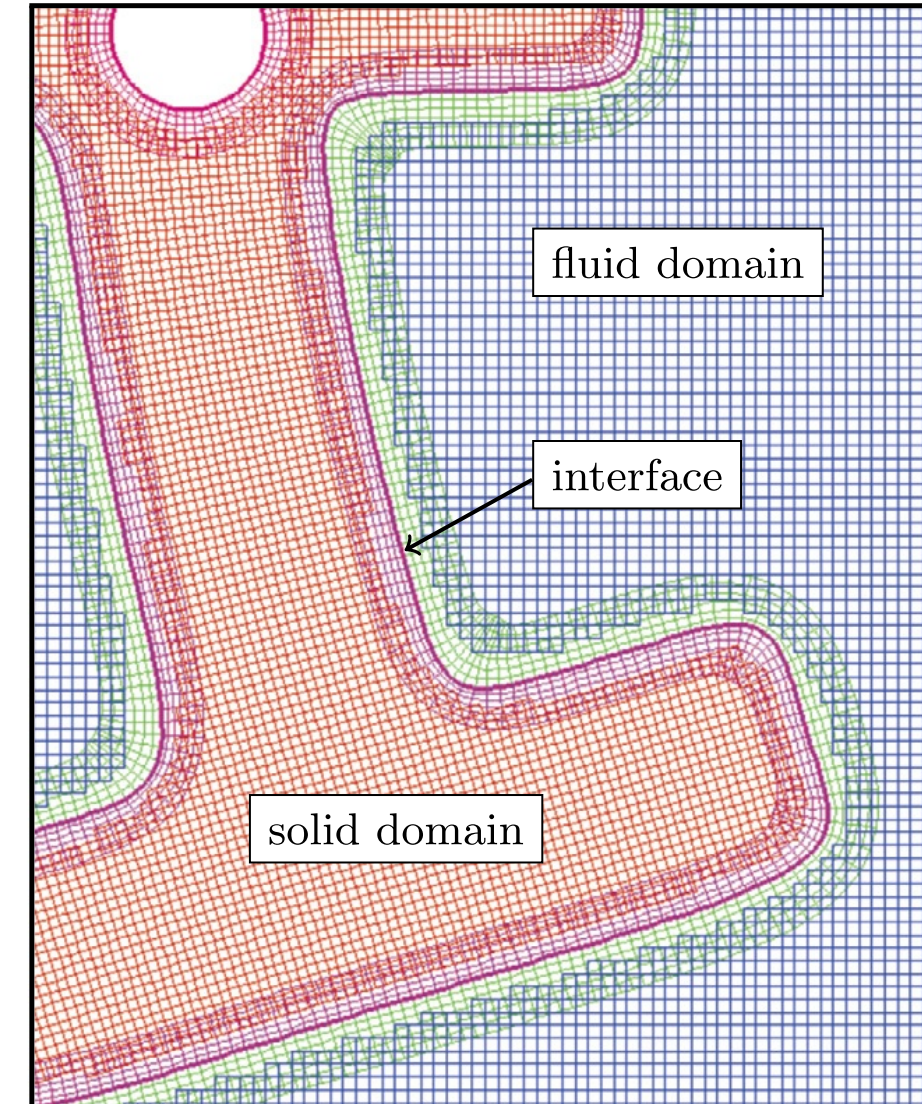
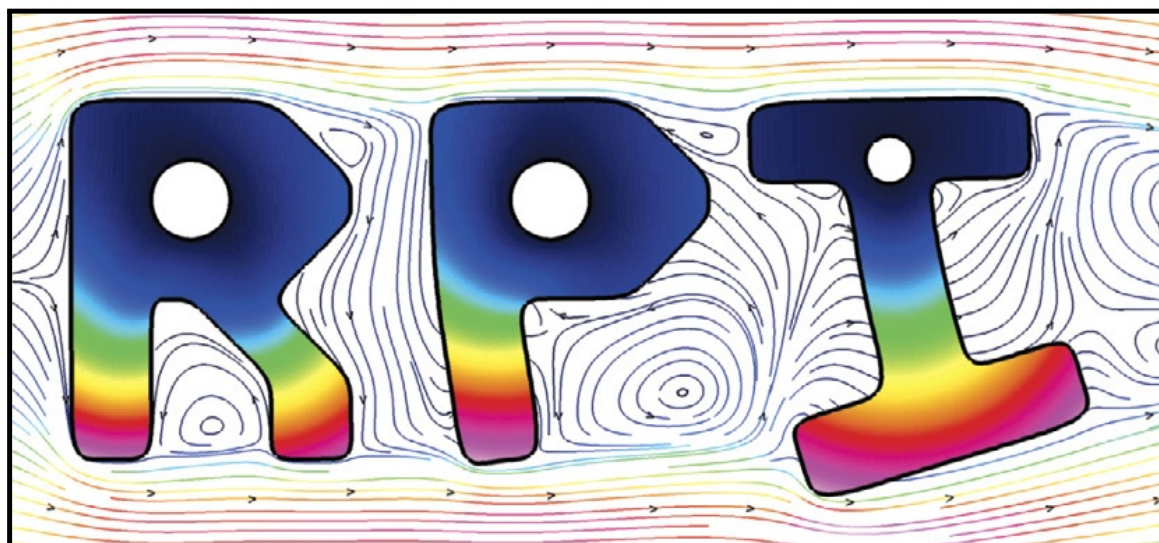
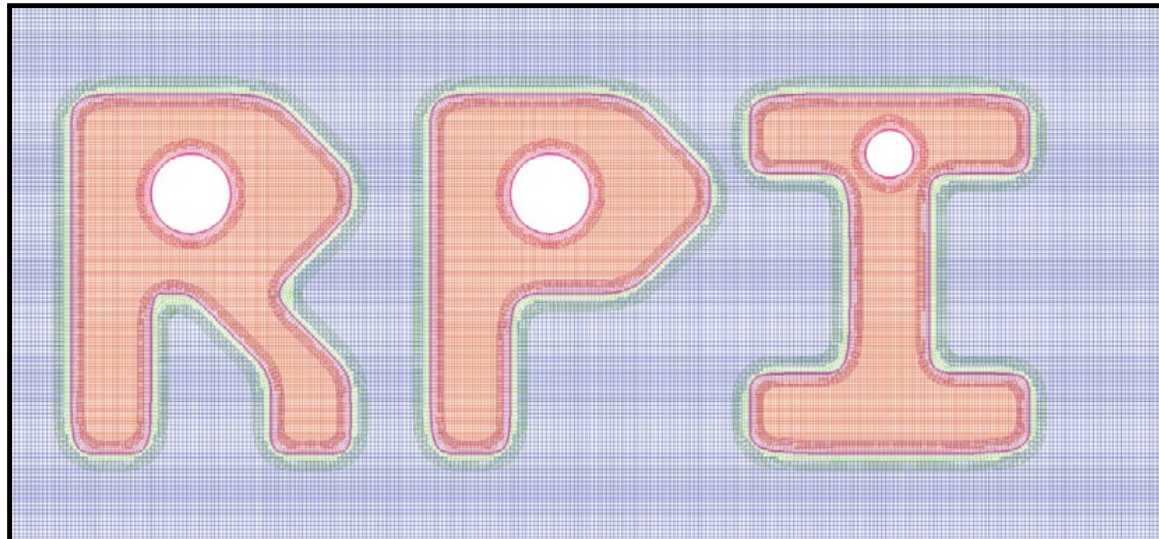
Time histories of rigid body



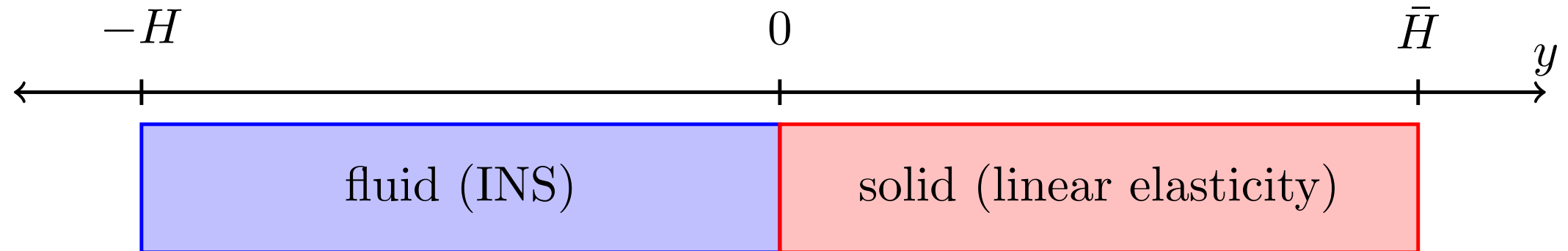
The AMP-FSI algorithm is very powerful and is stable for even the case of a zero mass rigid body



Compatibility coupling for incompressible FSI must deal with the complication of infinite propagation speed for the incompressibility constraint



Amazingly, the 1D problem can be used as a guide to develop the AMP scheme



velocity-pressure form

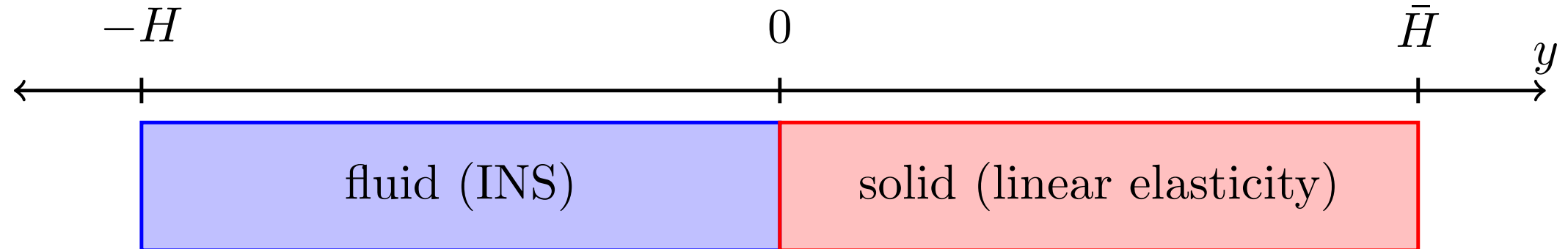
$$\begin{cases} \rho \partial_t v = -\partial_y p \\ \partial_{yy} p = 0 \end{cases}$$

$$\begin{cases} \partial_t \bar{u} - \bar{v} = 0 \\ \bar{\rho} \partial_t \bar{v} - \partial_y \bar{\sigma} = 0 \\ \partial_t \bar{\sigma} - \bar{\rho} c_p^2 \partial_y \bar{v} = 0 \end{cases}$$

Interface Coupling Conditions

$$\begin{cases} v(0, t) = \bar{v}(0, t) \\ -p(0, t) = \bar{\sigma}(0, t) \end{cases}$$

Along the interface one can combine the fluid momentum and solid characteristic to give a mixed boundary condition for the fluid stress



- The fluid momentum is integrated in time

$$v^I(t) - v^I(t - \delta) = -\frac{1}{\rho} \int_{t-\delta}^t \partial_y p^I(\eta) d\eta$$

- The characteristic relation in the solid gives

$$\sigma^I(t) + \bar{z}v^I(t) = \bar{\sigma} + \bar{z}\bar{v}$$

- Combining these yields a mixed-integral type boundary condition for the stress

$$-p^I(t) - \frac{\bar{z}}{\rho} \int_{t-\delta}^t \partial_y p^I(\eta) d\eta = \bar{\sigma} + \bar{z}(\bar{v} - v^I(t - \delta))$$

The AMP scheme is found to be stable under the usual time-step constraint

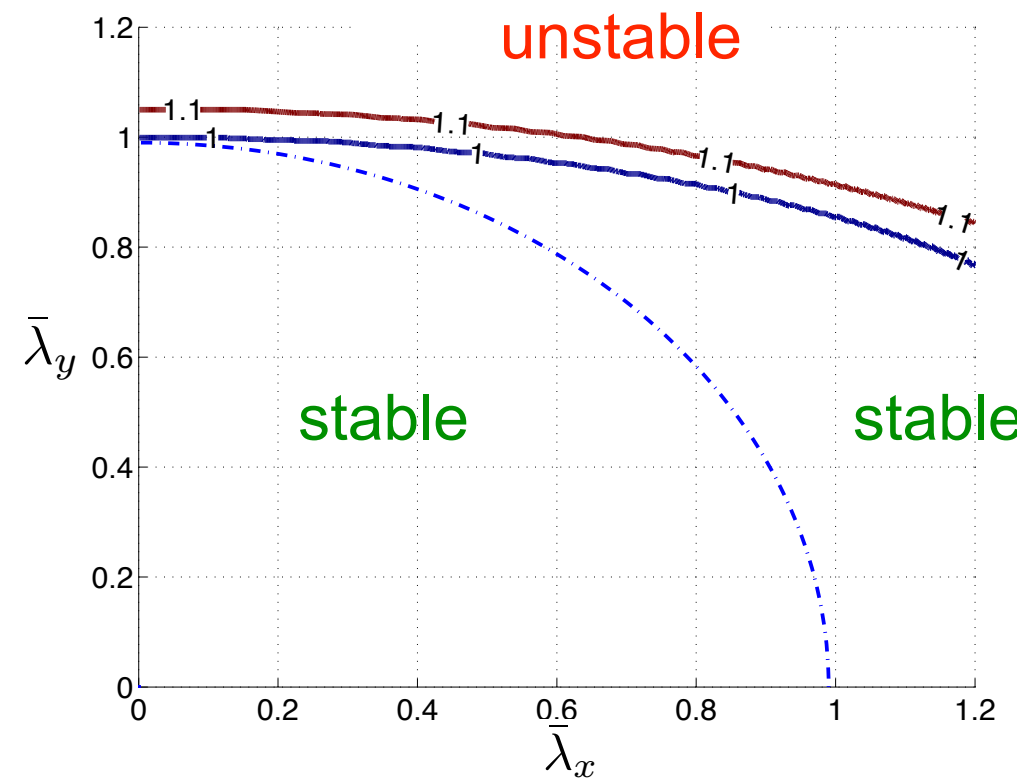
Theorem: The first-order upwind scheme for the solid, and the AMP algorithm

$$-p^{I,n+1} - \frac{\bar{z}_p \Delta t}{\rho} \partial_y p^{I,n+1} = \bar{\sigma}_{22}^{n+1} + \bar{z}_p (\bar{v}_2^{n+1} - v_2^{I,n})$$

$$v_2^{I,n+1} = \gamma v_2^{n+1} + \frac{1-\gamma}{\bar{z}_p} (\bar{z}_p \bar{v}_2^{n+1} + \bar{\sigma}_{22}^{n+1} + p^{I,n+1})$$

is stable for all material parameters provided $\bar{\lambda}_x^2 + \bar{\lambda}_y^2 \leq 1$ and $0 \leq \gamma < 2$

- Velocity weighting is used to avoid ill-conditioning in limiting cases



$$\bar{\lambda}_x = \bar{c}_p k_x \Delta t$$

$$\bar{\lambda}_y = \frac{\bar{c}_p \Delta t}{\Delta y}$$

The traditional scheme is found to be formally unconditionally unstable!

Theorem: The first-order upwind scheme for the solid, and traditional interface approximation

$$v_2^{I,n+1} = \bar{v}_2^{n+1}$$

$$p^{I,n+1} = -p^{n+1}$$

$$\text{is stable if and only if } \Delta t \leq \frac{2}{\bar{c}_p} \left(\Delta y - \frac{\rho L}{\bar{\rho}} \right)$$

- Therefore the traditional scheme is unstable if the mass of the solid in a single cell is less than the mass of the entire fluid domain
- For coarse meshes the scheme may appear stable, but for sufficiently fine grids the scheme will experience exponential blowup
- This is a worst case of the 2D analysis

Interestingly, the anti-traditional scheme is found to be formally stable

Theorem: The first-order upwind scheme for the solid, and anti- traditional interface approximation

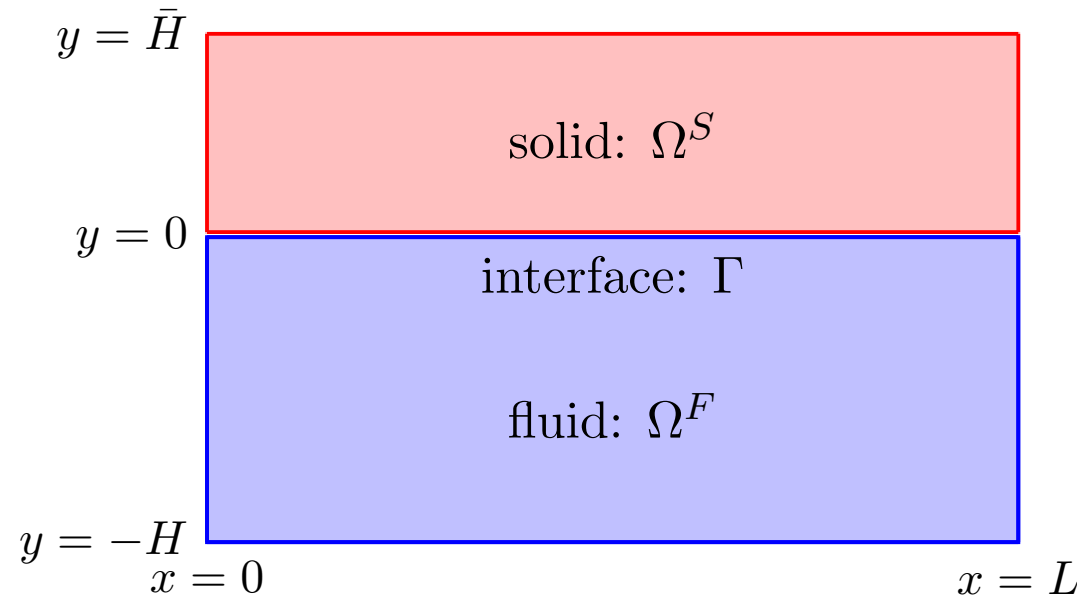
$$v_2^{I,n+1} = v_2^{n+1}$$

$$p^{I,n+1} = -\bar{\sigma}_{22}^{n+1}$$

is stable if and only if $\Delta t \leq \frac{\Delta y}{\bar{c}_p} \left(\sqrt{\mathcal{M}^2 + 8\mathcal{M}} - \mathcal{M} \right)$, where $\mathcal{M} = \frac{\rho H}{\bar{\rho} \Delta y}$

- Therefore the anti-traditional scheme is stable if the time step is taken small enough
- For the heavy solid regime however, the stable time step may be impractically small
- Note that there are apparently no instances of this anti-traditional scheme in the literature

In more complex settings, compatibility coupling reveals “interesting” mathematical structure



$$\text{Fluid: } \begin{cases} \rho \frac{\partial \mathbf{v}}{\partial t} + \nabla p = \mu \Delta \mathbf{v}, \\ \nabla \cdot \mathbf{v} = 0, \\ \mathbf{v}(x, -H, t) = 0 \end{cases}$$

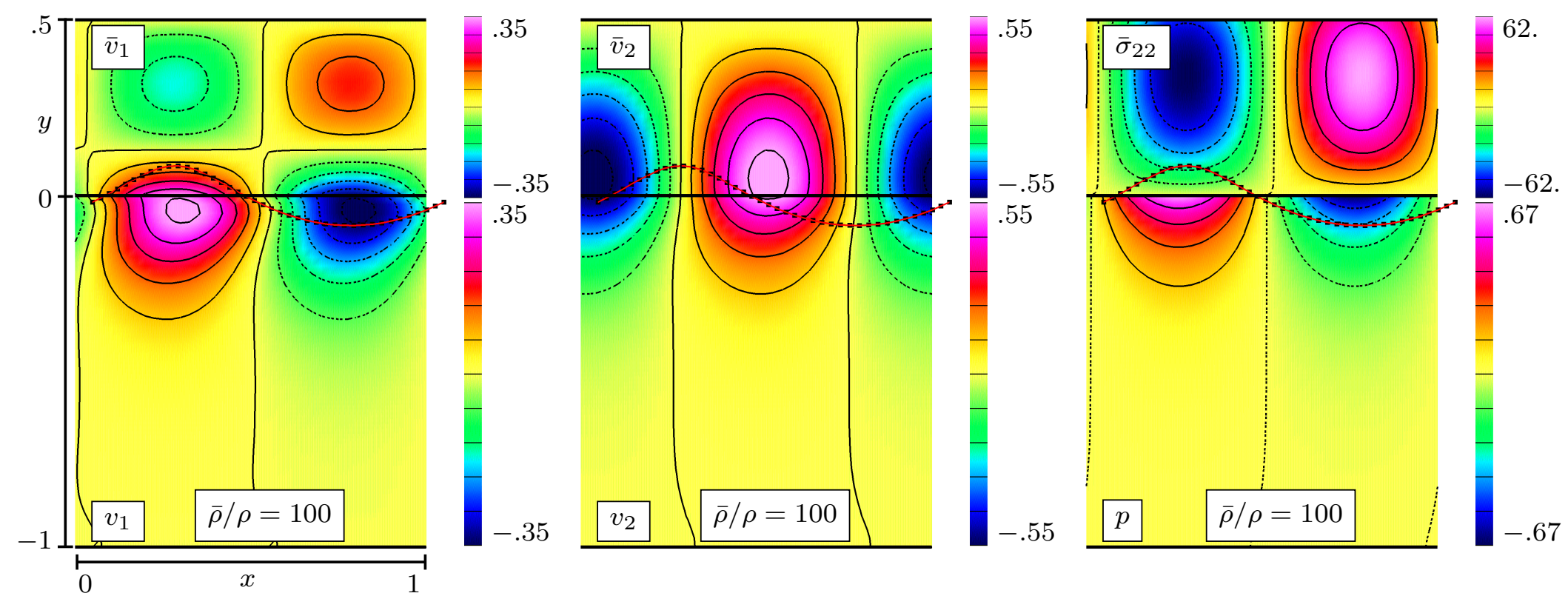
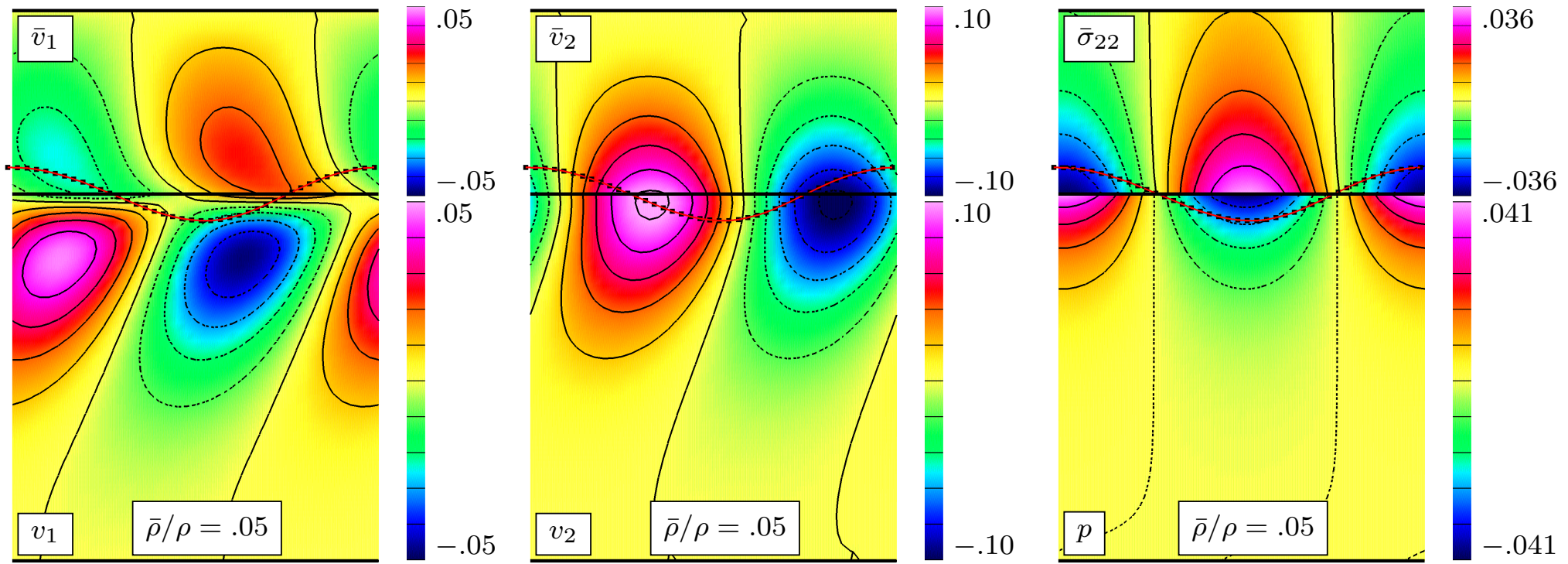
$$\text{Solid: } \begin{cases} \bar{\rho} \frac{\partial^2 \bar{\mathbf{u}}}{\partial t^2} = (\bar{\lambda} + \bar{\mu}) \nabla (\nabla \cdot \bar{\mathbf{u}}) + \bar{\mu} \Delta \bar{\mathbf{u}}, \\ \bar{\mathbf{u}}(x, \bar{H}, t) = 0 \end{cases}$$

$$\text{Interface: } \mathbf{v} = \frac{\partial \bar{\mathbf{u}}}{\partial t}, \quad \mu \left(\frac{\partial v_1}{\partial y} + \frac{\partial v_2}{\partial x} \right) = \bar{\mu} \left(\frac{\partial \bar{u}_1}{\partial y} + \frac{\partial \bar{u}_2}{\partial x} \right), \quad -p + 2\mu \frac{\partial v_2}{\partial y} = \bar{\lambda} \nabla \cdot \bar{\mathbf{u}} + 2\bar{\mu} \frac{\partial \bar{u}_2}{\partial y}$$

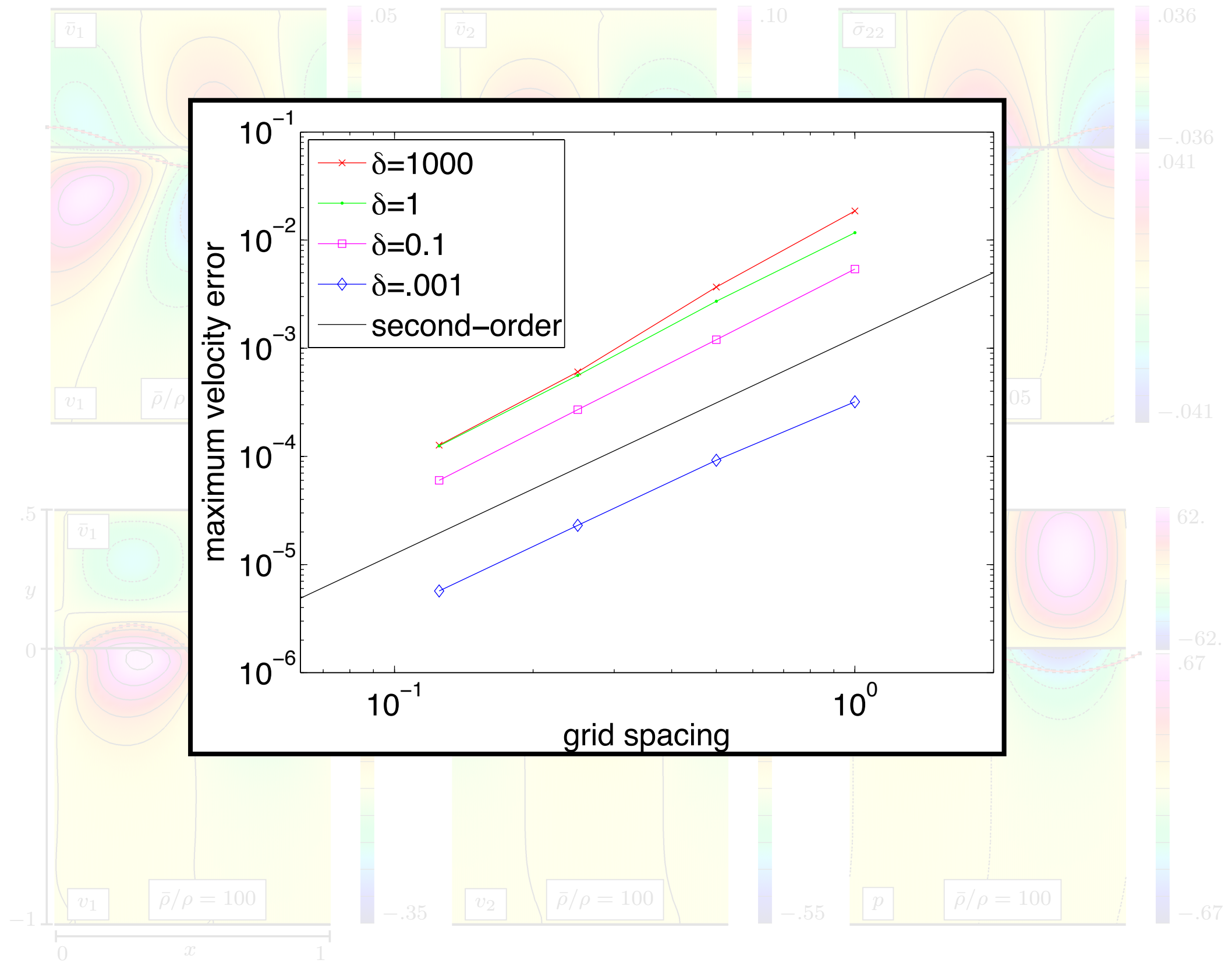
- The AMP interface condition for the pressure is

$$-p - \frac{\bar{z}_p \Delta t}{\rho} \frac{\partial p}{\partial n} = -\mathbf{n}^T \boldsymbol{\tau} \mathbf{n} + \frac{\mu \bar{z}_p \Delta t}{\rho} \mathbf{n}^T (\nabla \times \nabla \times \mathbf{v}) + \mathbf{n}^T \bar{\boldsymbol{\sigma}} \mathbf{n} + \bar{z}_p \Delta t \mathbf{n}^T \frac{\partial \bar{\mathbf{v}}}{\partial t}$$

Exact traveling wave solutions for Stokes flow and linear elastic solids are used to demonstrate stability and second-order accuracy for the AMP scheme in 2D



Exact traveling wave solutions are used to demonstrate stability and second-order accuracy for the AMP scheme in 2D



For this same 2D problem, the traditional scheme is shown to exhibit instability as the mesh is refined, as predicted by the theory

MP-VE, traveling wave, TP algorithm				
h_j	$\bar{\rho}/\rho = 800$	$\bar{\rho}/\rho = 400$	$\bar{\rho}/\rho = 200$	$\bar{\rho}/\rho = 100$
1/20	stable	stable	stable	stable
1/40	stable	stable	stable	unstable
1/80	stable	stable	unstable	unstable
1/160	stable	unstable	unstable	unstable
1/320	unstable	unstable	unstable	unstable

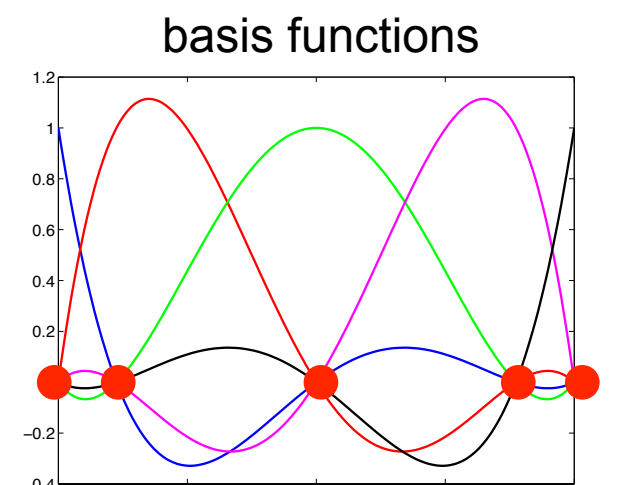
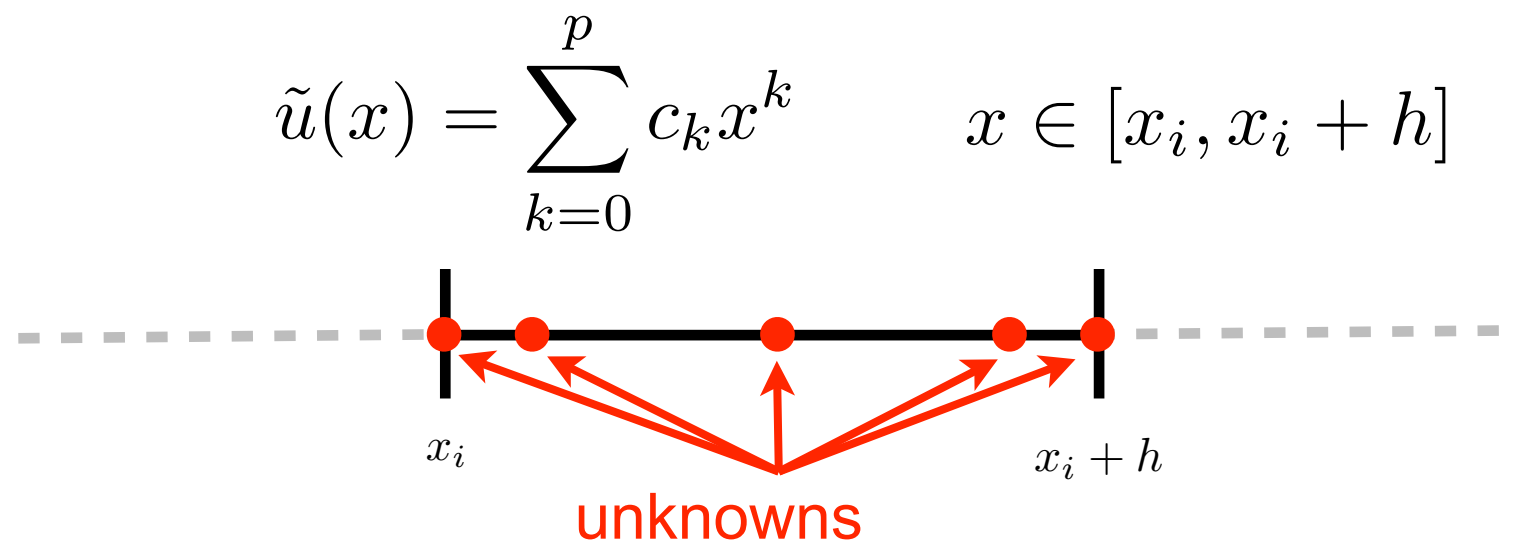
We have also considered the AMP scheme for the nonlinear incompressible Navier Stokes equations coupled to rigid solids



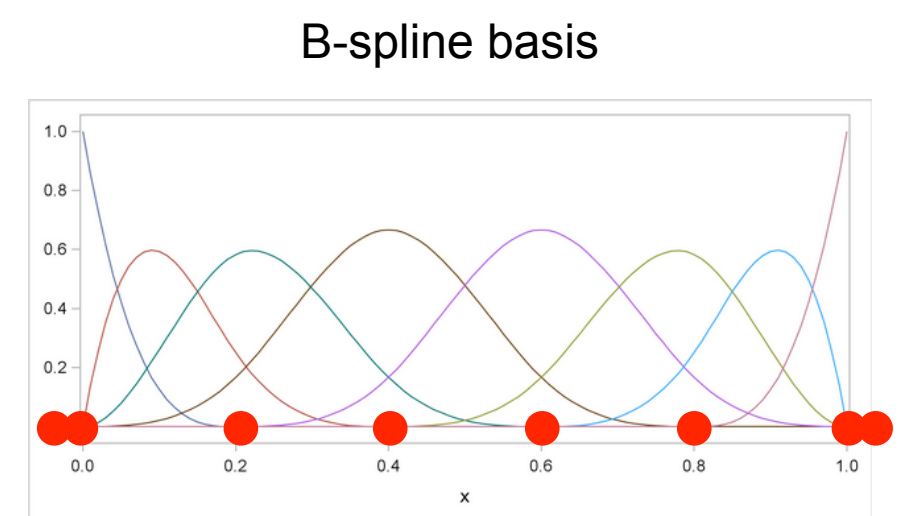
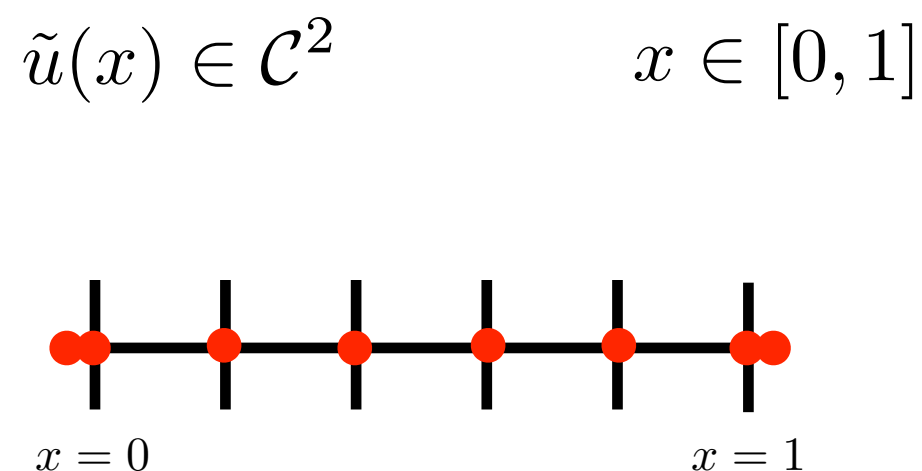
- Here we find strong added-mass and added-damping effects, and the AMP projection is formulated to address both
- Again, second-order accuracy in max norm is demonstrated using MMS and through self convergence studies

The non-standard operators arising in compatibility-based coupling may be challenging in the context of energy stable weak-form methods

- On one end of the spectrum are p-refinement methods that introduce interior degrees of freedom (Solin et. al. 2004, Hesthaven and Warburton (2008)

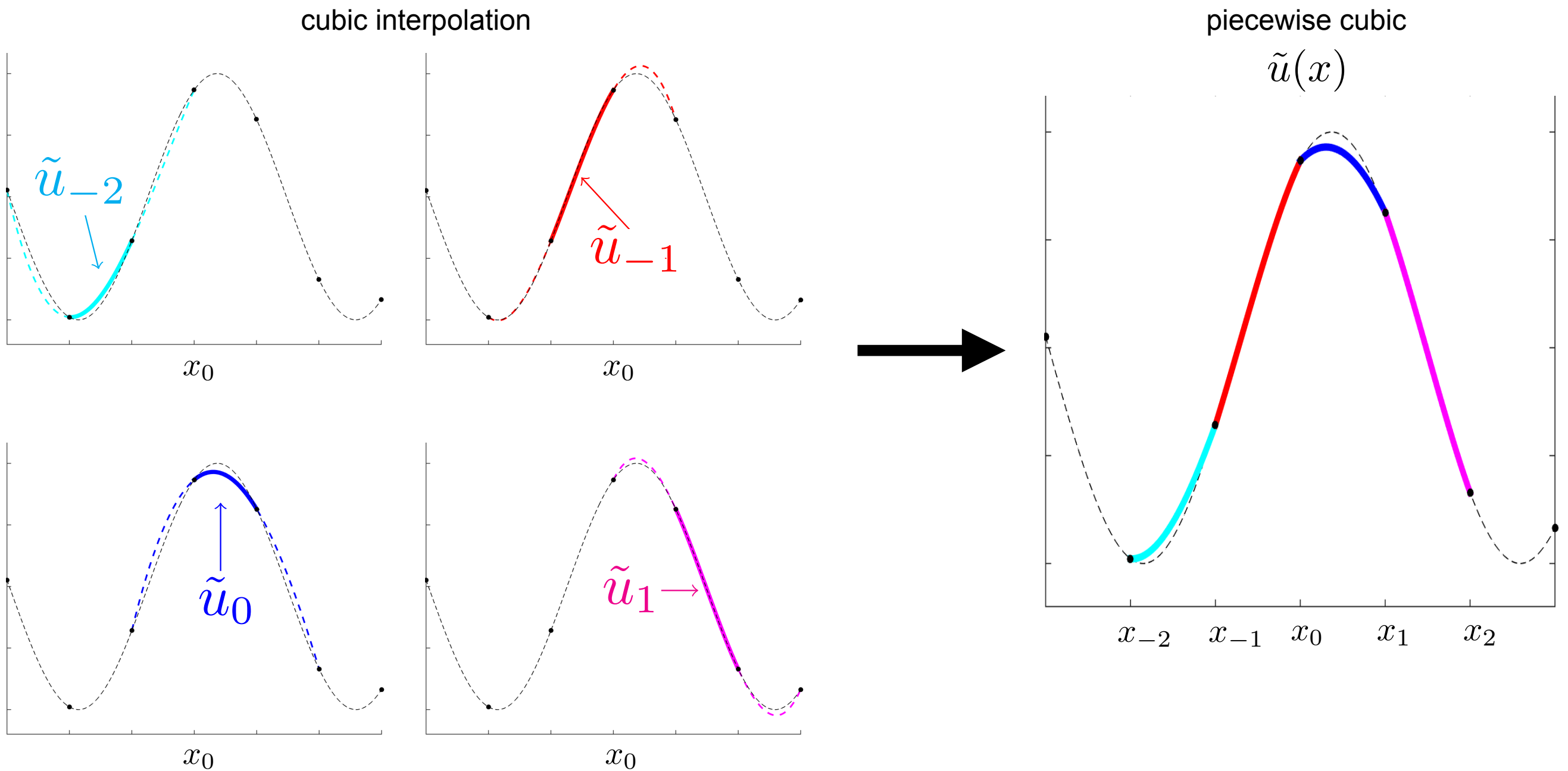


- On the other end of the spectrum are spline based methods that impose high-order continuity but do not introduce interior DOFs (Hughes et. al. 2005)



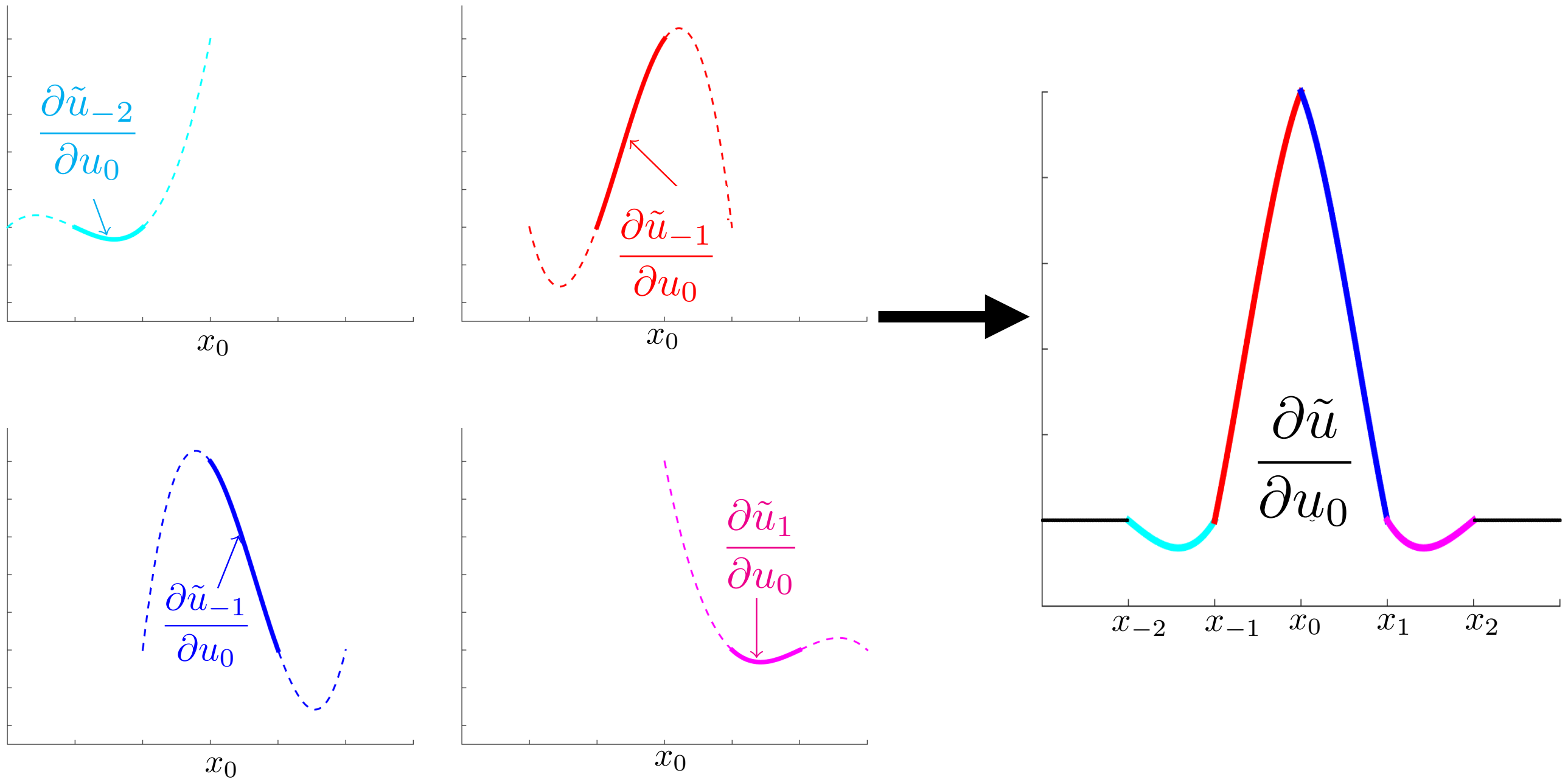
There is a relatively unstudied intermediate approach which uses neighbor data rather than interior DOFs or globalizing high-order continuity constraints

- Over each interval we define a local reconstruction that interpolates data beyond the interval where the definition is valid (Kormann 2012)



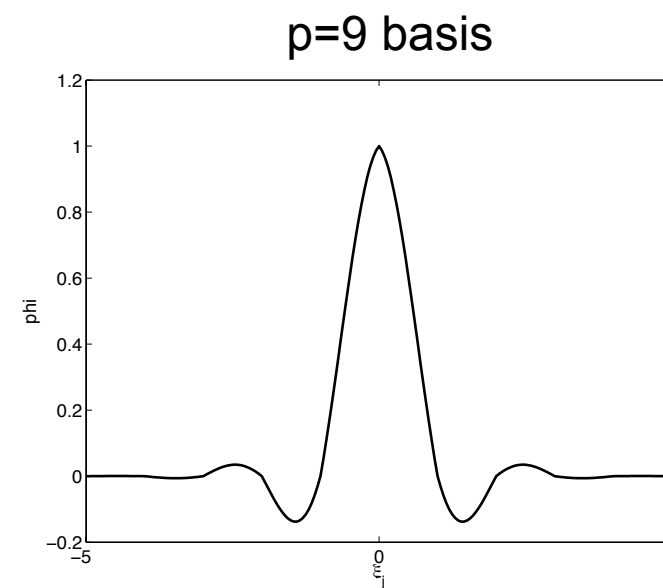
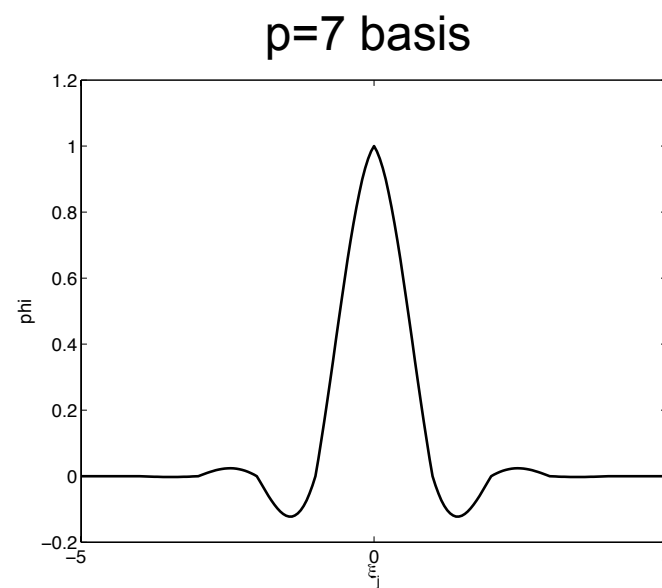
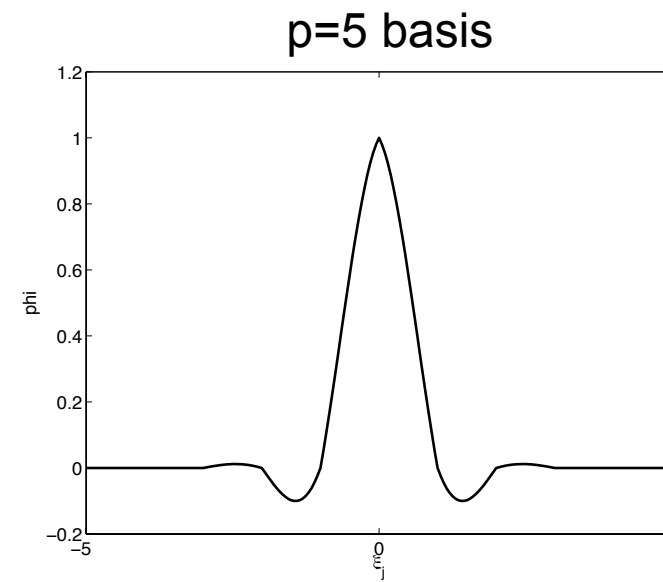
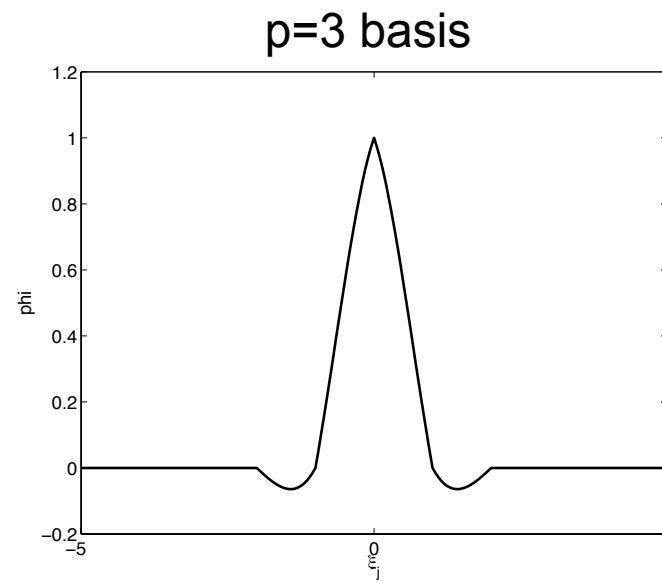
There is a relatively unstudied intermediate approach which uses neighbor data rather than interior DOFs or globalizing high-order continuity constraints

- Over each interval we define a local reconstruction that interpolates data beyond the interval where the definition is valid (Kormann 2012)
- Basis functions can be associated with each unknown $\phi_j^{(p)}(x) = \frac{\partial}{\partial u_j} \tilde{u}(x)$



There is a relatively unstudied intermediate approach which uses neighbor data rather than interior DOFs or globalizing high-order continuity constraints

- Over each interval we define a local reconstruction that interpolates data beyond the interval where the definition is valid (Kormann 2012)
- Basis functions can be associated with each unknown $\phi_j^{(p)}(x) = \frac{\partial}{\partial u_j} \tilde{u}(x)$
- Extension to higher-order basis functions is straightforward



Using this basis we can pursue discretization using standard variational techniques

- The solution takes the form

$$\tilde{u}(x) = \sum_j u_j \phi_j^{(p)}(x)$$

- Ignoring boundaries for a moment and using the notation $(v, w) = \int vw dx$

$$(\psi, u_{xx}) = -(\psi_x, u_x)$$

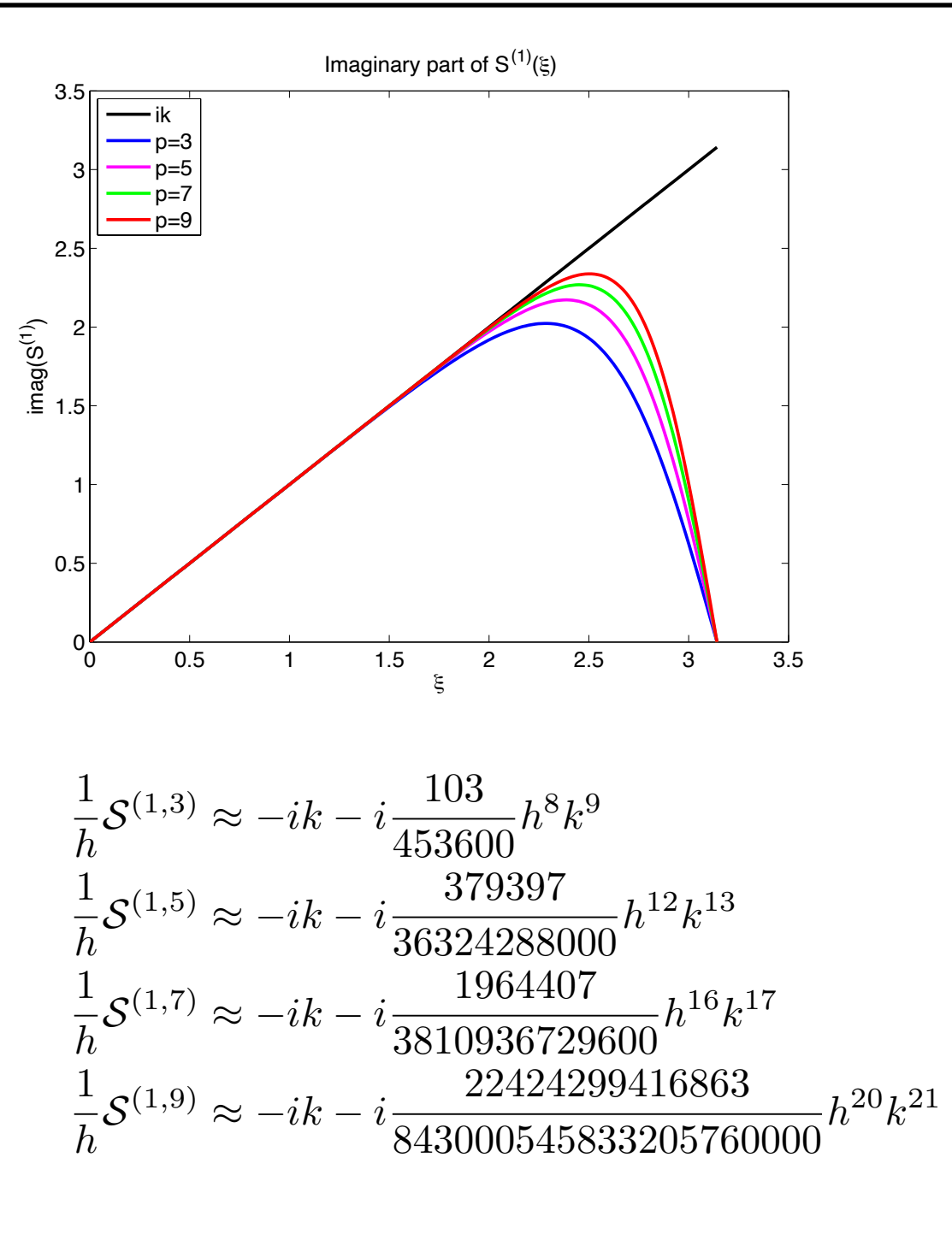
$$\sum_{\alpha=-p}^p M_\alpha^{(p)} u_{xxj+\alpha} = \sum_{\alpha=-p}^p K_\alpha^{(2,p)} u_{j+\alpha}$$

- The discrete Fourier spectrum can found by assuming $u_j = \exp(ikx)$

$$-k^2 = \frac{\sum_{\alpha=-p}^p K_\alpha^{(2,p)} \exp(i\alpha\xi)}{\sum_{\alpha=-p}^p M_\alpha^{(p)} \exp(i\alpha\xi)} \equiv \frac{1}{h^2} \mathcal{S}^{(1,p)}(\xi)$$

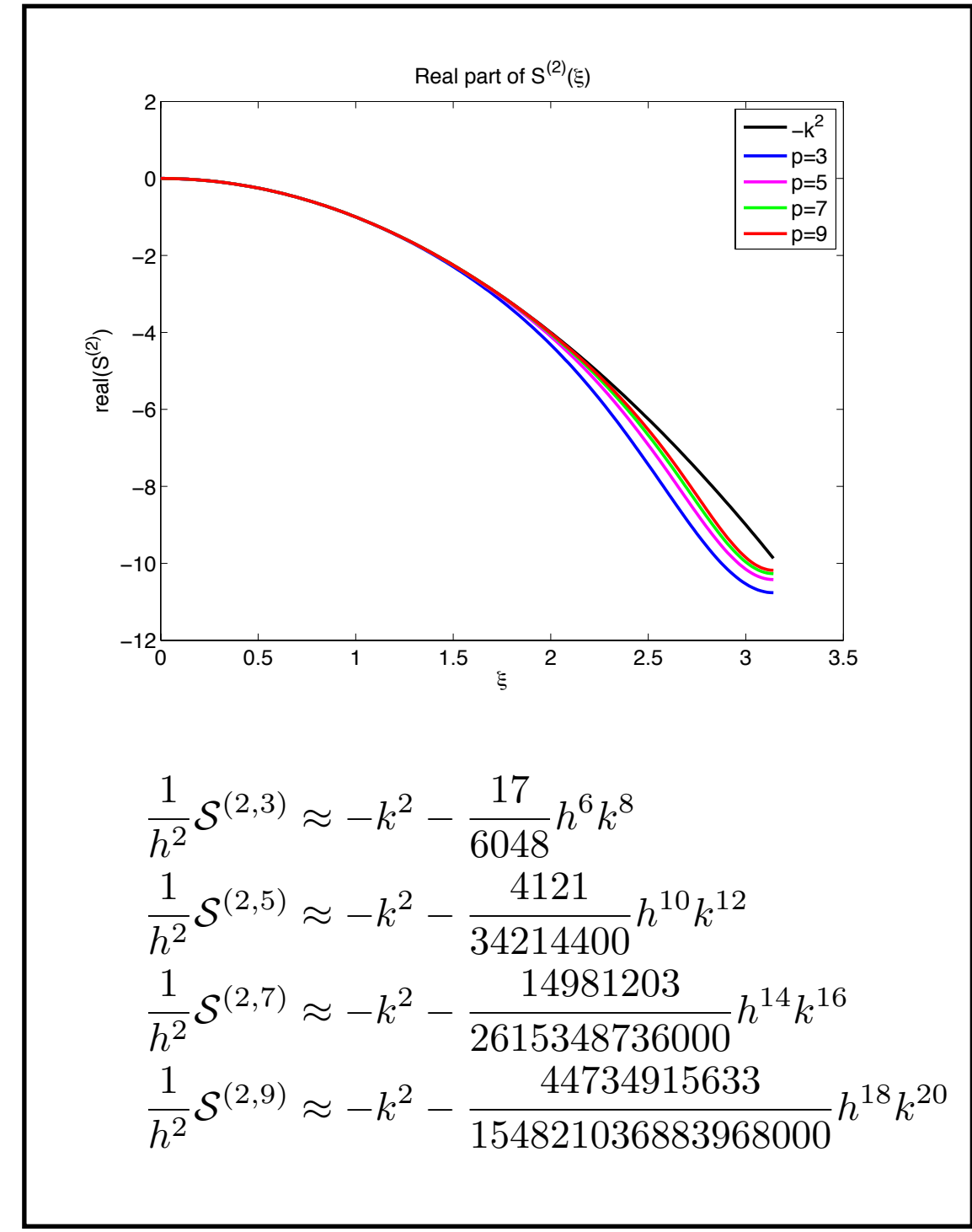
The approximations are found to be extremely accurate and have bounded stiffness with increasing order

$$\frac{\partial}{\partial x}$$



$$\begin{aligned} \frac{1}{h} \mathcal{S}^{(1,3)} &\approx -ik - i \frac{103}{453600} h^8 k^9 \\ \frac{1}{h} \mathcal{S}^{(1,5)} &\approx -ik - i \frac{379397}{36324288000} h^{12} k^{13} \\ \frac{1}{h} \mathcal{S}^{(1,7)} &\approx -ik - i \frac{1964407}{3810936729600} h^{16} k^{17} \\ \frac{1}{h} \mathcal{S}^{(1,9)} &\approx -ik - i \frac{22424299416863}{843000545833205760000} h^{20} k^{21} \end{aligned}$$

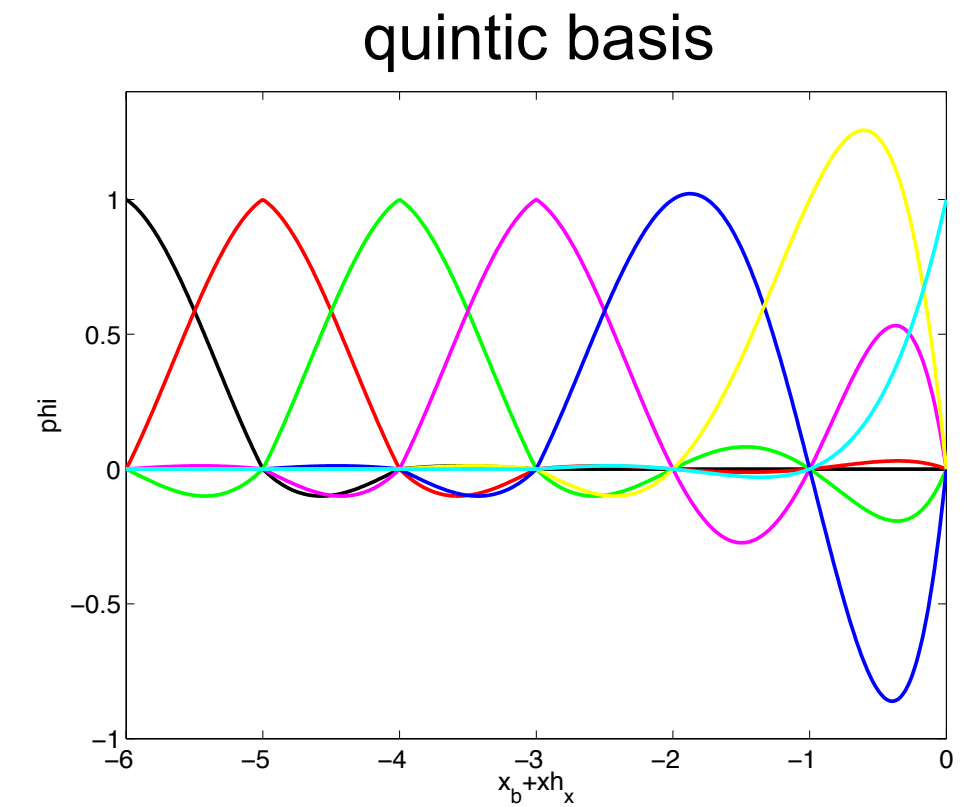
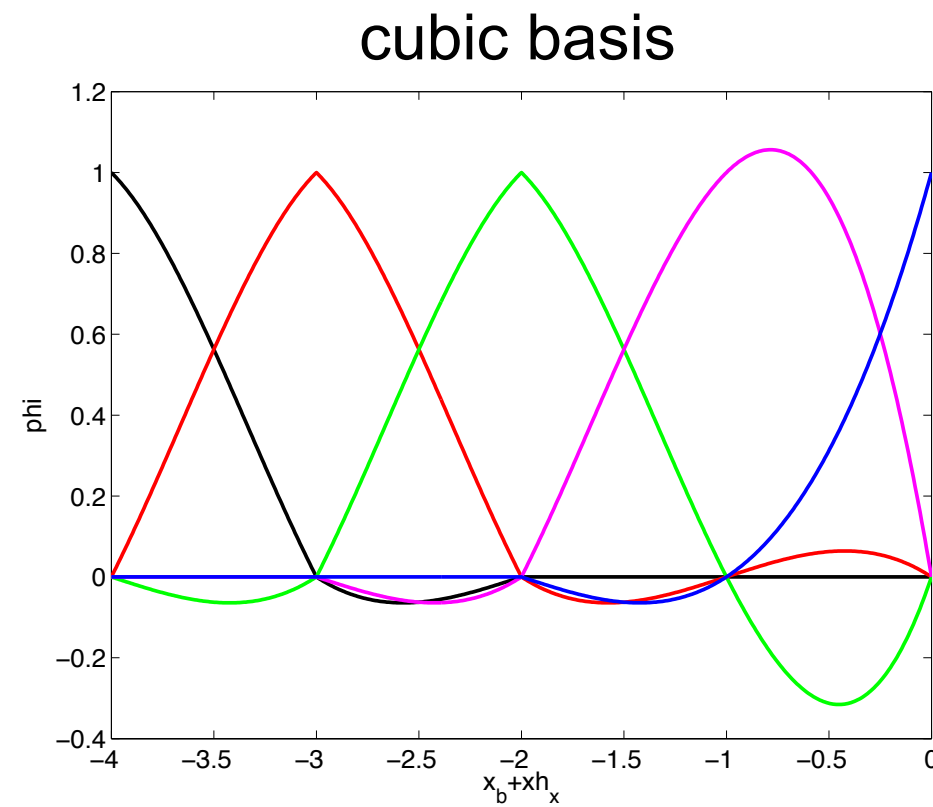
$$\frac{\partial^2}{\partial^2 x}$$



$$\begin{aligned} \frac{1}{h^2} \mathcal{S}^{(2,3)} &\approx -k^2 - \frac{17}{6048} h^6 k^8 \\ \frac{1}{h^2} \mathcal{S}^{(2,5)} &\approx -k^2 - \frac{4121}{34214400} h^{10} k^{12} \\ \frac{1}{h^2} \mathcal{S}^{(2,7)} &\approx -k^2 - \frac{14981203}{2615348736000} h^{14} k^{16} \\ \frac{1}{h^2} \mathcal{S}^{(2,9)} &\approx -k^2 - \frac{44734915633}{154821036883968000} h^{18} k^{20} \end{aligned}$$

Generic boundary closures can be obtained by employing one-sided interpolation or through the use of ghost cells similar to BCs in FD methods

- Extrapolation is straightforward and follows essentially the same logic as traditional FEM near boundaries. This can be viewed as a modification to the basis functions.



- Alternately additional degrees of freedom can be retained in “ghost cells” while the discrete solution and all integrals are still taken over the physical domain interior

Boundary closures based on compatibility boundary conditions remove stiffness associated with one-sided closures, but are specific to the PDE and BC

- e.g. consider the scalar wave equation with Neumann BC

$$\bar{\rho} \frac{\partial^2 \bar{u}}{\partial t^2} = c^2 \frac{\partial^2 \bar{u}}{\partial x^2}$$

$$\frac{\partial \bar{u}}{\partial x}(x_b, t) = 0$$

- Repeated differentiation of the BC in time and use of the governing equation yields

$$\frac{\partial^3 \bar{u}}{\partial x \partial t^2}(x_b, t) = c^2 \frac{\partial^3 \bar{u}}{\partial x^3}(x_b, t) = 0$$

$$\frac{\partial^5 \bar{u}}{\partial x \partial t^4}(x_b, t) = c^4 \frac{\partial^5 \bar{u}}{\partial x^5}(x_b, t) = 0$$

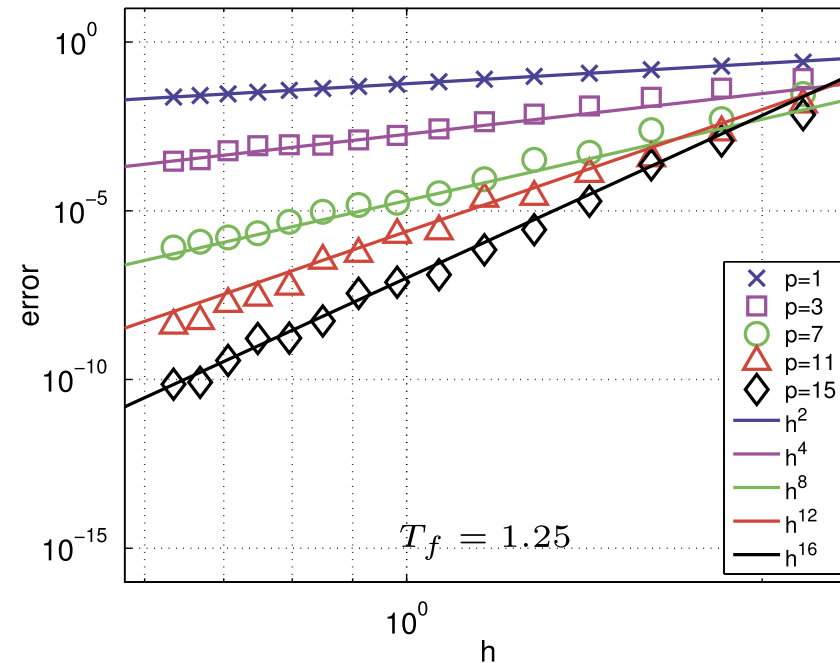
$$\frac{\partial^7 \bar{u}}{\partial x \partial t^6}(x_b, t) = c^6 \frac{\partial^7 \bar{u}}{\partial x^7}(x_b, t) = 0$$

⋮

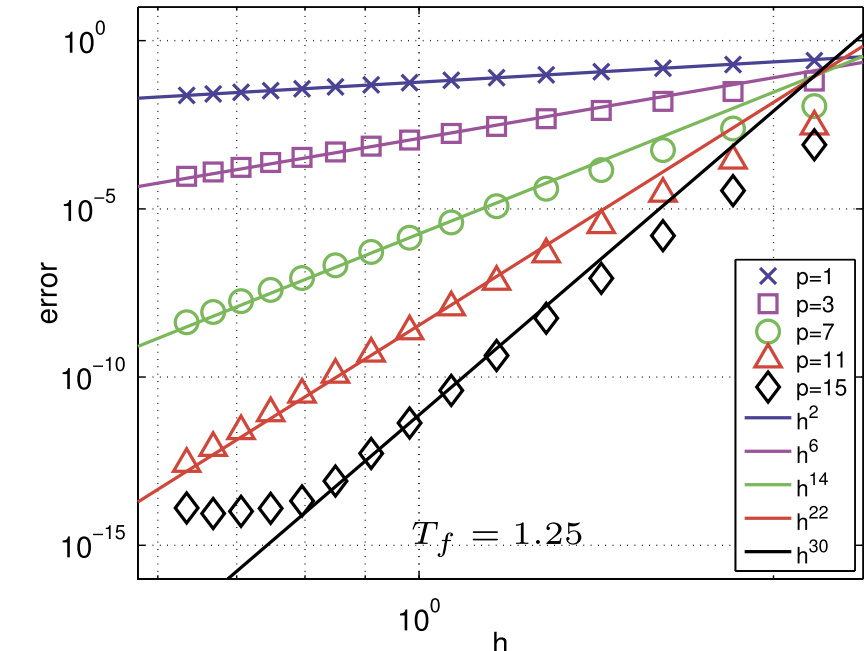
The observed convergence rates often exceeds the theoretical prediction of $p+1$, and often approach the superconvergent rate of $2p$

- e.g. consider the scalar wave equation in 2D

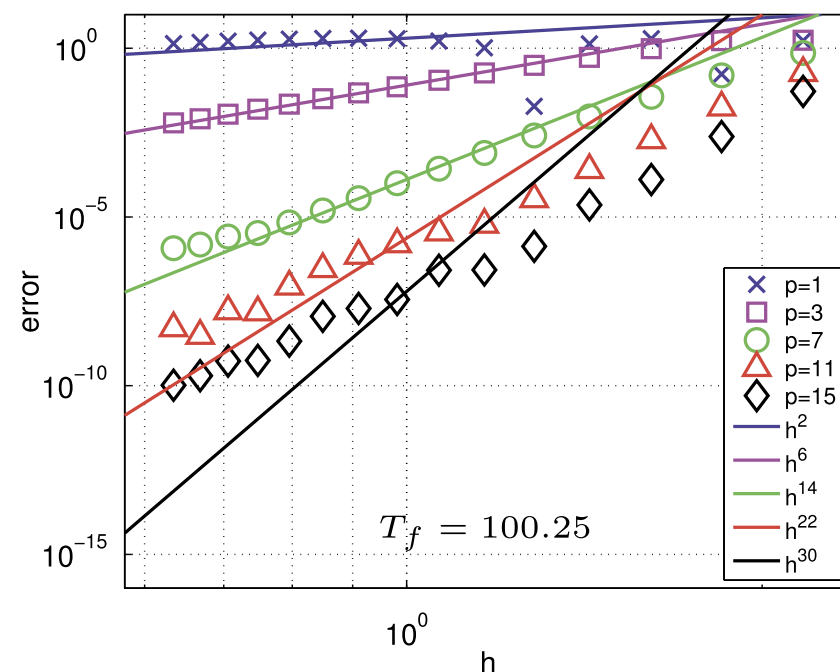
extrapolation



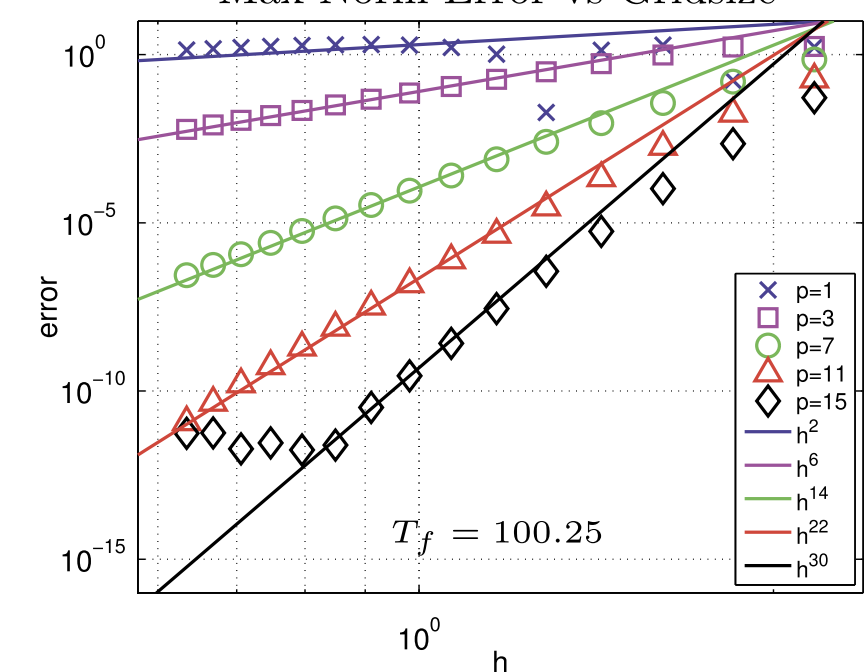
compatibility



Max Norm Error vs Gridsize

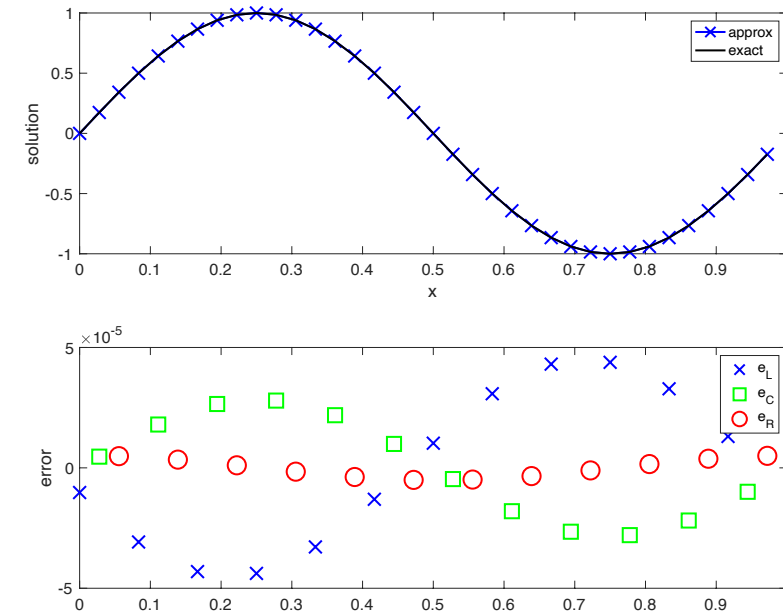
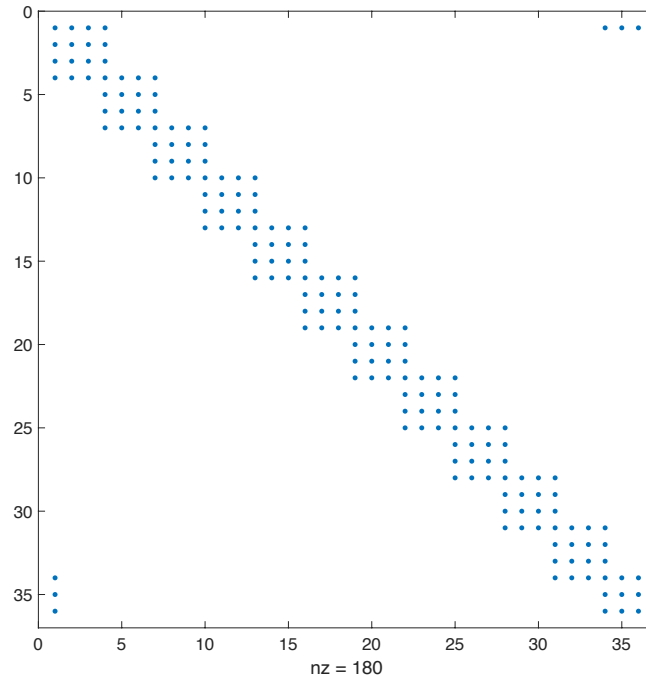


Max Norm Error vs Gridsize

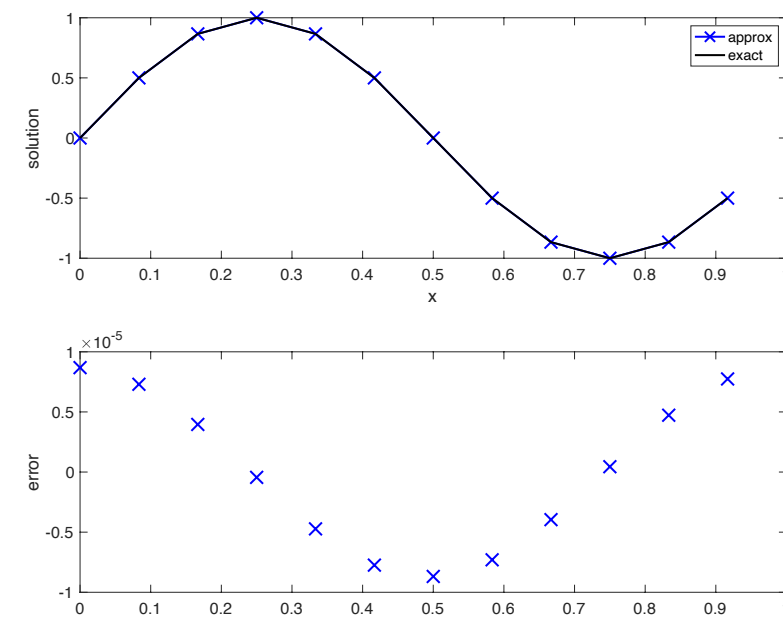
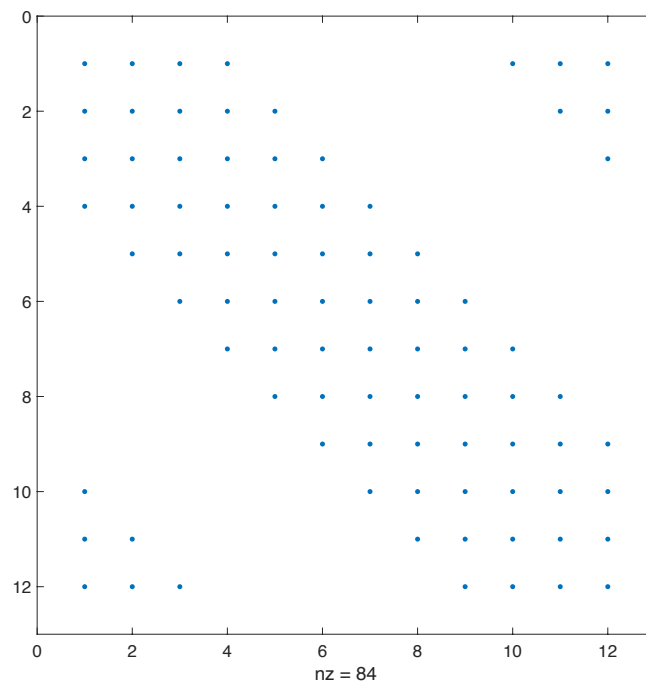


GD can be thought of as a projection from “standard” FEM, e.g. $u_t + au_x = 0$

- Classical cubic continuous FEM with 12 elements (36 DoFs)

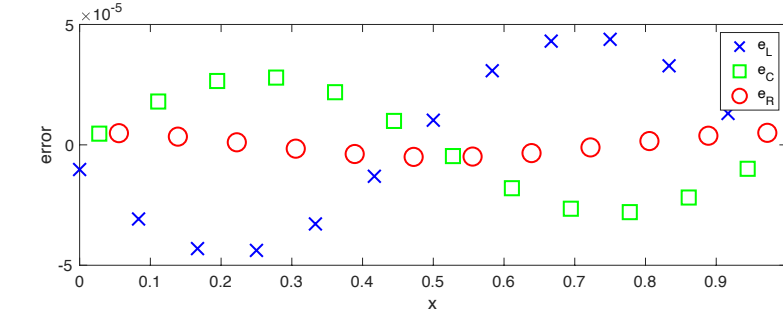
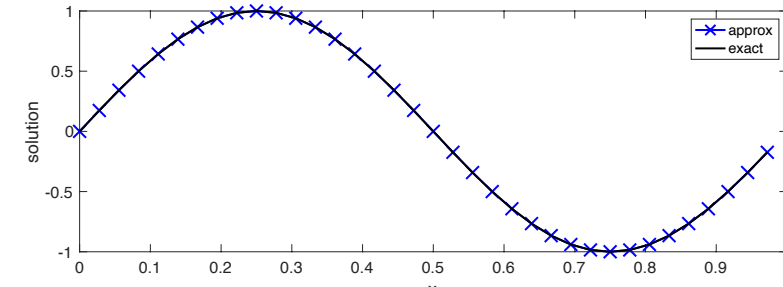
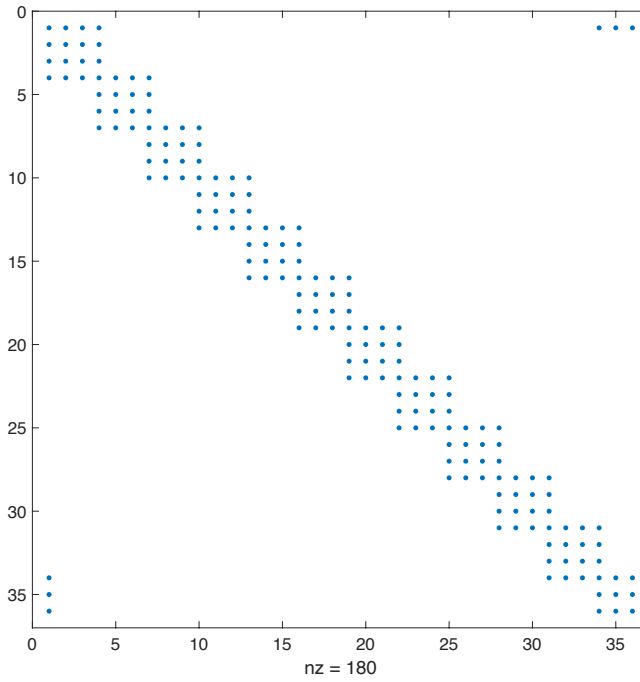


- GD with 12 “elements” (12 DoFs)

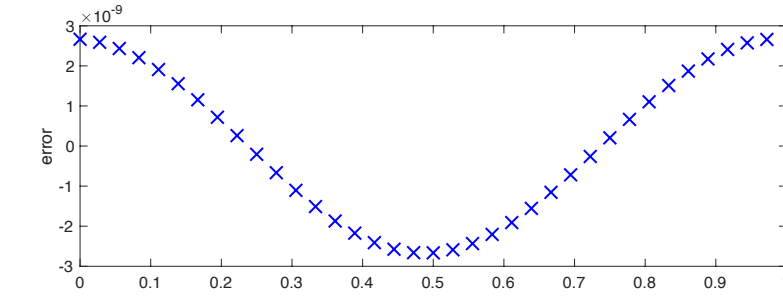
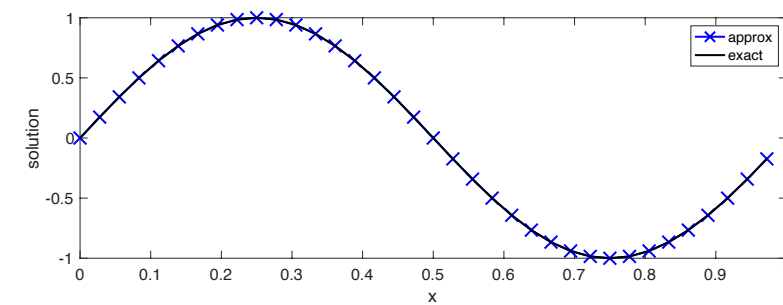
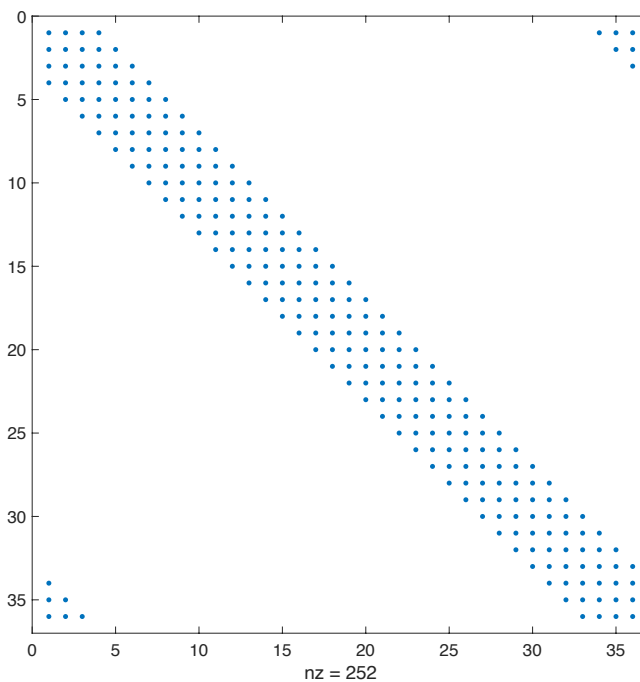


GD can be thought of as a projection from “standard” FEM, e.g. $u_t + au_x = 0$

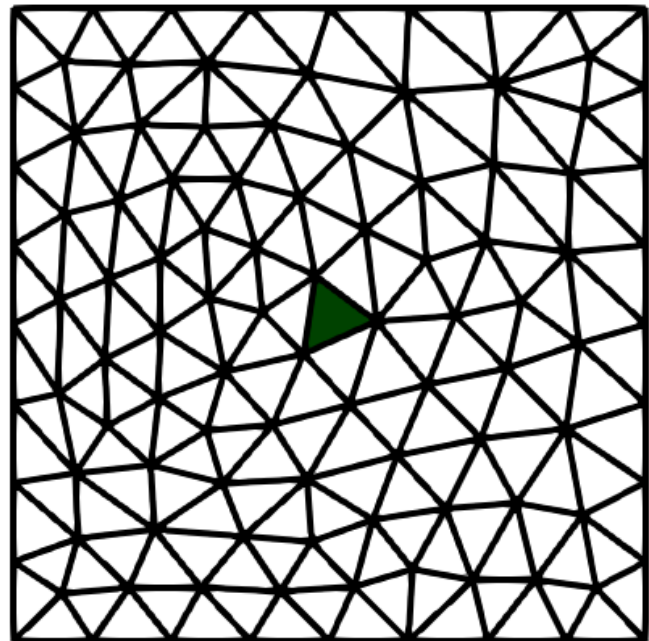
- Classical cubic continuous FEM with 12 elements (36 DoFs)



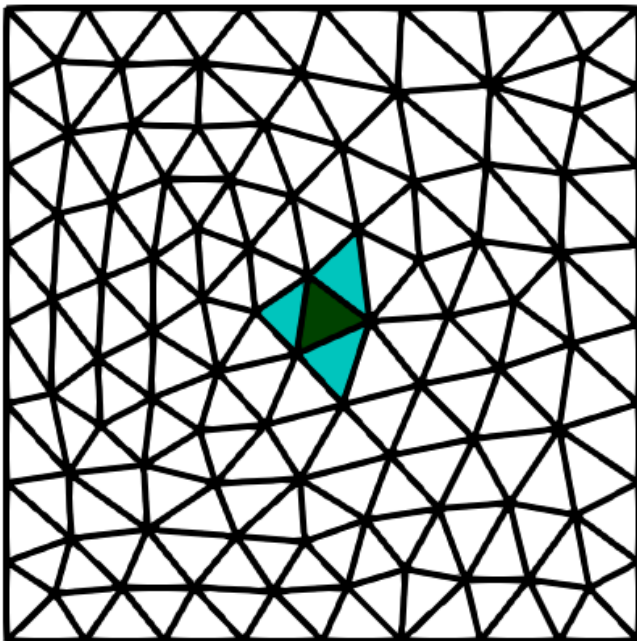
- GD with 36 “elements” (36 DoFs)



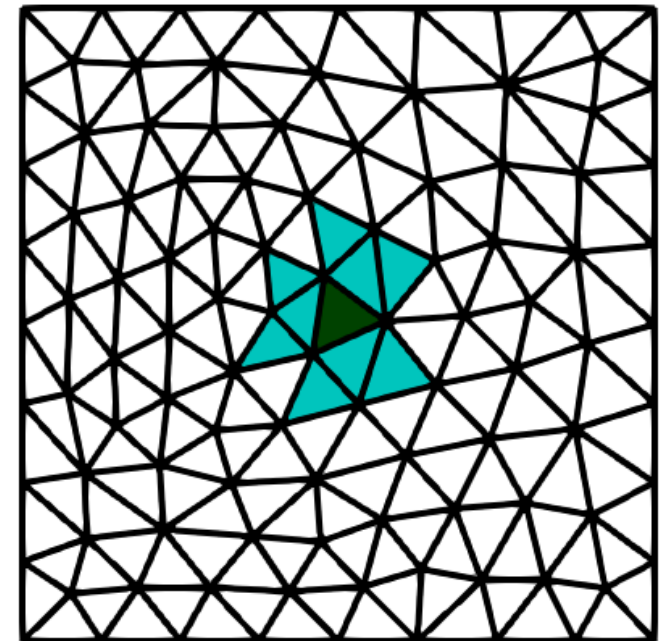
For unstructured grids, a least squares interpolant is used to define the basis and the GD operators can be formed using projection from SPB-scheme (in MFEM)



p=0

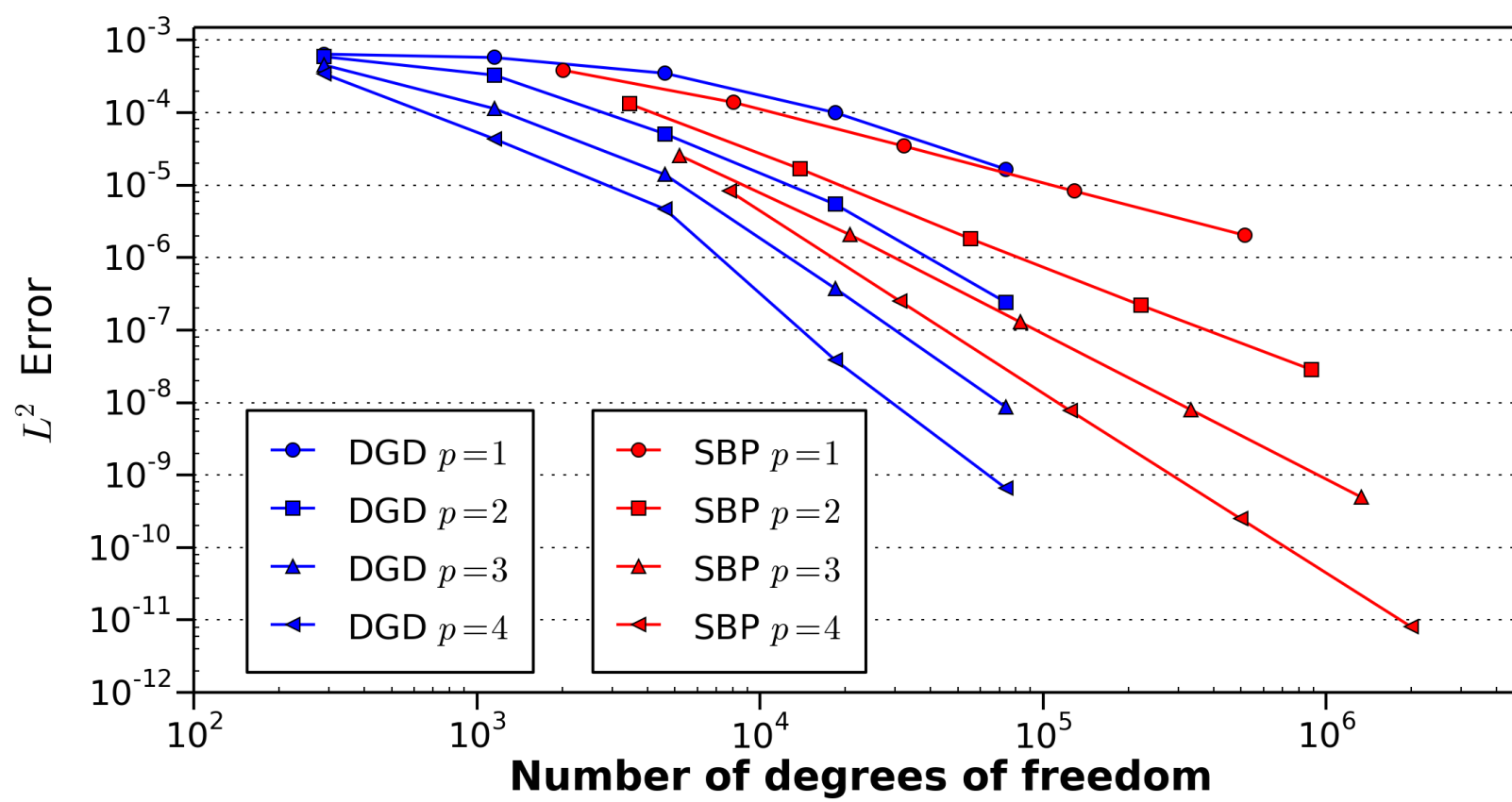
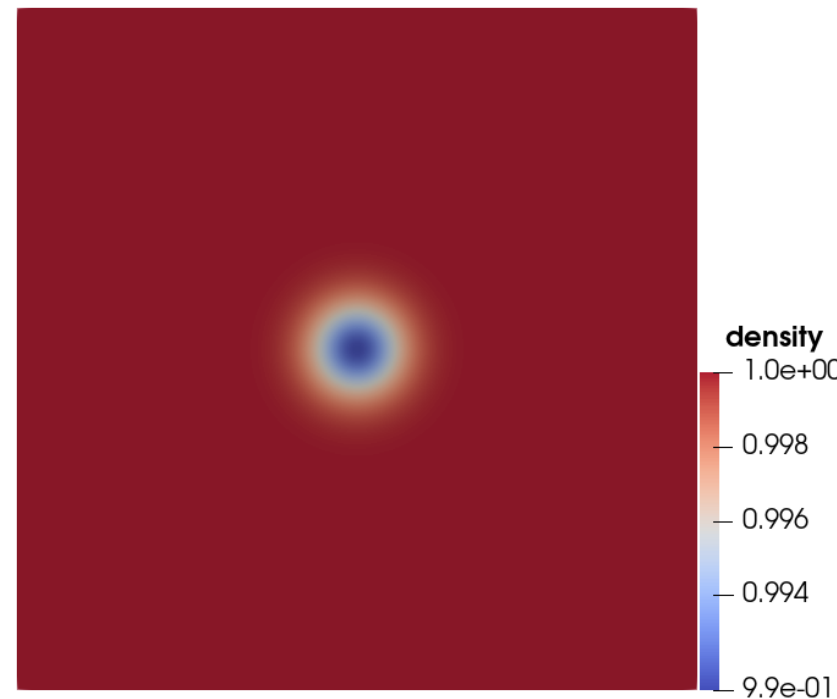


p=1



p=2

An unsteady isentropic vortex case illustrates that GD may outperform standard variational schemes in terms of error per DoF



Summary

- I have discussed our compatibility-based AMP schemes for FSI
- Moving toward FEM, I have developed GD schemes that accommodate CBCs
- We have briefly seen the relation between GD and classical FEM

Future Work

- New FSI regimes (incompressible/incompressible, compressible/beams)
- Other multidomain regimes (acoustics, EM, etc ...)
- GD-based solvers for FSI using CBCs